

## Article (refereed) - postprint

---

Sanczuk, Pieter; Verheyen, Kris; Lenoir, Jonathan; Zellweger, Florian; Lembrechts, Jonas J.; Rodríguez-Sánchez, Francisco; Baeten, Lander; Bernhardt-Römermann, Markus; De Pauw, Karen; Vangansbeke, Pieter; Perring, Michael P. ; Berki, Imre; Bjorkman, Anne D.; Brunet, Jörg; Chudomelová, Markéta; De Lombaerde, Emiel; Decocq, Guillaume; Dirnböck, Thomas; Durak, Tomasz; Greiser, Caroline; Hédli, Radim; Heinken, Thilo; Jandt, Ute; Jaroszewicz, Bogdan; Kopecký, Martin; Landuyt, Dries; Macek, Martin; Máliš, František; Naaf, Tobias; Nagel, Thomas A.; Petřík, Petr; Reczyńska, Kamila; Schmidt, Wolfgang; Standovár, Tibor; Staude, Ingmar R.; Świerkosz, Krzysztof; Teleki, Balázs; Vanneste, Thomas; Vild, Ondrej; Waller, Donald; De Frenne, Pieter. 2024. **Unexpected westward range shifts in European forest plants link to nitrogen deposition.**

Copyright © 2024 The Authors, some rights reserved.

This version is available at <http://nora.nerc.ac.uk/id/eprint/538254>

Copyright and other rights for material on this site are retained by the rights owners. Users should read the terms and conditions of use of this material at <https://nora.nerc.ac.uk/policies.html#access>

**This is the author's version of the work. The definitive version was published in Science 386 (6718): 193-198, 11 October 2024, DOI: <https://doi.org/10.1126/science.ado0878>**

**This is the final manuscript version incorporating any revisions agreed during the peer review process. There may be differences between this and the publisher's version. You are advised to consult the publisher's version if you wish to cite from this article.**

The definitive version is available at <https://science.sciencemag.org>

Contact UKCEH NORA team at  
[noraceh@ceh.ac.uk](mailto:noraceh@ceh.ac.uk)

# Unexpected westward range shifts in European forest plants link to nitrogen deposition

Pieter Sanczuk<sup>1\*</sup>, Kris Verheyen<sup>1</sup>, Jonathan Lenoir<sup>2</sup>, Florian Zellweger<sup>3</sup>, Jonas J. Lembrechts<sup>4,5</sup>, Francisco Rodriguez-Sanchez<sup>5</sup>, Lander Baeten<sup>1</sup>, Markus Bernhardt-Römermann<sup>7,8</sup>, Karen De Pauw<sup>1</sup>, Pieter Vangansbeke<sup>1</sup>, Michael P. Perring<sup>9,10</sup>, Imre Berki<sup>11</sup>, Anne Bjorkman<sup>12,13</sup>, Jörg Brunet<sup>14</sup>, Markéta Chudomelová<sup>15</sup>, Emiel De Lombaerde<sup>1†</sup>, Guillaume Decocq<sup>2</sup>, Thomas Dirnböck<sup>16</sup>, Tomasz Durak<sup>17</sup>, Caroline Greiser<sup>18,19</sup>, Radim Hédli<sup>15,20</sup>, Thilo Heinken<sup>20</sup>, Ute Jandt<sup>22,23</sup>, Bogdan Jaroszewicz<sup>24</sup>, Martin Kopecký<sup>25,26</sup>, Dries Landuyt<sup>1</sup>, Martin Macek<sup>25</sup>, František Máliš<sup>27,28</sup>, Tobias Naaf<sup>29</sup>, Thomas A. Nagel<sup>30</sup>, Petr Petřík<sup>31,32</sup>, Kamila Reczyńska<sup>33</sup>, Wolfgang Schmidt<sup>34</sup>, Tibor Standovár<sup>35</sup>, Ingmar Staude<sup>23,36</sup>, Krzysztof Świerkosz<sup>37</sup>, Balázs Teleki<sup>38</sup>, Thomas Vanneste<sup>1</sup>, Ondrej Vild<sup>15</sup>, Donald Waller<sup>39</sup>, Pieter De Frenne<sup>1</sup>

\*corresponding author: Pieter Sanczuk ; [Pieter.Sanczuk@UGent.be](mailto:Pieter.Sanczuk@UGent.be)

## Affiliations:

<sup>1</sup>Forest & Nature Lab, Department of Environment, Ghent University, Melle-Gontrode, Belgium

<sup>2</sup>UMR CNRS 7058 "Ecologie et dynamique des systèmes anthropisés" (EDYSAN), Université de Picardie Jules Verne, Amiens Cedex 1, France

<sup>3</sup>Forest Resources and Management, Swiss Federal Research Institute WSL, Birmensdorf, Switzerland

<sup>4</sup>Research Center on Plants and Ecosystems (PLECO), University of Antwerp, Wilrijk, Belgium

<sup>5</sup>Ecology & Biodiversity (E&B), Utrecht University, Utrecht, the Netherlands

<sup>6</sup>Universidad de Sevilla, Departamento de Biología Vegetal y Ecología, Sevilla, Spain

<sup>7</sup>Friedrich Schiller University Jena, Institute of Ecology and Evolution, Jena, Germany

<sup>8</sup>iDiv, German Centre for Integrative Biodiversity Research (iDiv) Halle-Jena-Leipzig, Leipzig, Germany

<sup>9</sup>Environment Centre Wales, UKCEH (UK Centre for Ecology and Hydrology), Bangor, UK

<sup>10</sup>The UWA Institute of Agriculture, The University of Western Australia, Perth, Australia

<sup>11</sup>Faculty of Forestry, Institute of Environmental and Earth Sciences, University of Sopron, Sopron, Hungary

<sup>12</sup>Department of Biological and Environmental Sciences, University of Gothenburg, Gothenburg, Sweden

<sup>13</sup>Gothenburg Global Biodiversity Centre, Gothenburg, Sweden

<sup>14</sup>Southern Swedish Forest Research Centre, Swedish University of Agricultural Sciences, Lomma, Sweden

<sup>15</sup>Department of Vegetation Ecology, Institute of Botany of the Czech Academy of Sciences, Brno, Czech Republic

<sup>16</sup>Ecosystem Research and Environmental Information Management, Environment Agency Austria, Vienna, Austria

<sup>17</sup>Institute of Biology, University of Rzeszów, Rzeszów, Poland

<sup>18</sup>Department of Physical Geography, Stockholm University, Stockholm, Sweden

34 <sup>19</sup>Department of Forest Ecology and Management, Swedish University of Agricultural Sciences, Umeå,  
35 Sweden

36 <sup>20</sup>Department of Botany, Palacký University in Olomouc, Olomouc, Czech Republic

37 <sup>21</sup>Institute of Biochemistry and Biology, University of Potsdam, Potsdam, Germany

38 <sup>22</sup>Institute of Biology/Geobotany and Botanical Garden, Martin-Luther-University Halle-Wittenberg,  
39 Halle/Saale, Germany

40 <sup>23</sup>German Centre for Integrative Biodiversity Research (iDiv) Halle-Jena Leipzig, Leipzig, Germany

41 <sup>24</sup>Faculty of Biology, Białowieża Geobotanical Station, University of Warsaw, Białowieża, Poland

42 <sup>25</sup>Department of Geocology, Institute of Botany of the Czech Academy of Sciences, Průhonice, Czech  
43 Republic

44 <sup>26</sup>Faculty of Forestry and Wood Sciences, Czech University of Life Sciences Prague, Praha 6 - Suchbát,  
45 Czech Republic

46 <sup>27</sup>Department of Phytology, Technical University in Zvolen, Zvolen, Slovakia

47 <sup>28</sup>National Forest Centre, Zvolen, Slovakia

48 <sup>29</sup>Leibniz Centre for Agricultural Landscape Research (ZALF), Muencheberg, Germany

49 <sup>30</sup>Department of forestry and renewable forest resources, Biotechnical Faculty, University of Ljubljana,  
50 Ljubljana, Slovenia

51 <sup>31</sup>Department of vegetation ecology, Czech Academy of Sciences, Institute of Botany, Brno, Czech  
52 Republic

53 <sup>32</sup>Department of Ecology, Faculty of Environmental Sciences, Czech University of Life Sciences Prague,  
54 Czech Republic

55 <sup>33</sup>Independent Researcher, Wrocław, Poland

56 <sup>34</sup>Department of Silviculture and Forest Ecology of the Temperate Zones, University of Goettingen,  
57 Göttingen, Germany

58 <sup>35</sup>Department of Plant Systematics, Ecology and Theoretical Biology, Institute of Biology, ELTE Eötvös  
59 Loránd University, Budapest, Hungary

60 <sup>36</sup>Institute of Biology, Leipzig University, Leipzig, Germany

61 <sup>37</sup>Museum of Natural History, University of Wrocław, Wrocław, Poland

62 <sup>38</sup>HUN-REN-UD Biodiversity and Ecosystem Services Research Group, University of Debrecen,  
63 Debrecen, Hungary

64 <sup>39</sup>Botany, University of Wisconsin - Madison, Madison, USA

65 †present address: Research Institute for Nature and Forest, Brussels, Belgium

66 **Abstract:** Climate change is commonly assumed to induce species' range shifts towards the poles. Yet,  
67 other environmental changes may affect the geographical distribution of species in unexpected ways. Here  
68 we quantify multi-decadal shifts in the distribution of European forest plants, and link these shifts to key  
69 drivers of forest biodiversity change: climate change, atmospheric deposition (nitrogen and sulphur) and  
70 forest canopy dynamics. Surprisingly, westward distribution shifts were 2.6 times more likely than  
71 northward ones. Not climate change, but nitrogen-mediated colonization events, possibly facilitated by the  
72 recovery from past acidifying deposition, best explain westward movements. Biodiversity redistribution  
73 patterns appear complex and are more likely driven by the interplay among several environmental changes  
74 than due to the exclusive effects of climate change alone.

75 **Key words:** Acidification, atmospheric pollution, eutrophication, nitrogen deposition, climate change,  
76 conservation policy, isotherms, forestREplot, forest ecosystems, species range shifts, sulphur deposition,  
77 understorey plants

78 **One Sentence Summary:** Nitrogen deposition rather than climate change explains unexpected westward  
79 range centroid shifts of European forest plants

80 **Main text**

81 One of the most prominent biogeographical changes of the 21<sup>st</sup> century is the large-scale redistribution of  
82 plants and animals in response to changes in the climate system (1). Warming temperatures are causing  
83 many terrestrial species to move towards higher latitudes and elevations, resulting in a reordering of  
84 species' distributions (1–3) and the emergence of novel communities (4). Empirical evidence has been  
85 reported for a wide range of ecosystems and taxa - from poleward and upslope range shifts in temperate  
86 regions (5, 6) and high-latitude boreal biomes (7) to upslope shifts in mountain vegetation (8) – suggesting  
87 an emerging link with anthropogenic climate warming (2, 9).

88 According to the most recent global synthesis (1), terrestrial species are shifting towards higher latitudes at  
89 an average rate of 1.11 km year<sup>-1</sup>. This trend, however, lacks statistical significance, possibly because  
90 estimates are often blurred by variation in methodological attributes (1, 10). Alternatively, species'  
91 redistributions in geographical directions that are orthogonal (i.e., west-east oriented) or even inverse (e.g.,  
92 equatorward) to the moving isotherms are less likely to be detected from commonly studied range boundary  
93 shifts along thermal transects of latitude and elevation alone (11, 12). Indeed, other prominent  
94 environmental changes such as atmospheric (nitrogen and sulphur) deposition and forest disturbances show  
95 spatial patterns that are weakly correlated to the geographic direction of climate change (13–15), and can  
96 also influence demographic processes of colonization and local extinction (1, 12, 16). To what extent these  
97 other environmental changes are contributing to species range shifts remains largely unquantified (17–19).

98 Here we quantify the rate and geographic direction of range shifts in 266 European forest understory plant  
99 species using multi-decadal community data collected in mature forest stands across 2,954 resurveyed semi-  
100 permanent vegetation plots (20) (**Fig. 1A**). Plant community data were derived from baseline surveys  
101 recorded between 1933 and 1994 and paired resurveys carried out after the baseline surveys between 1987  
102 and 2017 (median [min – max] inter-survey interval: 39 [13 – 67] years). We quantified shifts of species'  
103 distributions within the spatial extent of the study area based on range centroids, i.e., the abundance-  
104 weighted geometric center of a species' distribution (**Fig. S1**). In contrast to the more frequent  
105 quantification of range boundary shifts at the trailing or leading edges, analyzing centroid shifts allow us  
106 to obtain more robust estimates of the magnitude and geographic direction of complex distribution shifts  
107 (6, 11, 21). This is important, because range shift estimates from leading and trailing edges alone are more  
108 prone to bias from stochastic processes or low sample sizes that may blur overall biogeographical trends  
109 (11).

110 **The rate and geographic direction of centroid shifts**

111 To calculate the centroid shift of each species, we first located the position of the abundance-weighted range  
112 centroid at the time of the baseline survey and the resurvey, and assessed the magnitude (i.e., the distance)  
113 and geographical direction (i.e., the bearing) of the centroid shift over time. Centroid shifts were expressed  
114 as the absolute shift rate ( $km\ year^{-1}$ ) as well as the projected south-north ( $km\ north\ year^{-1}$ ) and west-east  
115 ( $km\ east\ year^{-1}$ ) rate (schematically explained in **Fig. S1**). Centroid shifts were calculated for the 266 species  
116 that were recorded in  $\geq 1\%$  of the plots to increase robustness of the estimates. The directionality (i.e.,  
117 angular dispersion of the directions of centroids shifts) across all species was tested using the Rayleigh's  $r$   
118 coefficient, a circular regression coefficient which quantifies how uniform and isotropic the directions of  
119 shifts are (Rayleigh's  $r = 1$  if all species are moving in the same direction while Rayleigh's  $r = 0$  with  
120 random directional movements, i.e., anisotropic, meaning that directions of shifts can be drawn from a  
121 uniform circular distribution).

122 Species' centroid shifts were first compared to the velocity and direction of climate change realized over  
123 the course of the study period. Spatially explicit climate change velocities were calculated by climate  
124 analogue mapping (22, 23), an approach that is theoretically equivalent to the mapping of species centroid  
125 shifts (**Fig. S1**). In contrast to the frequent calculation of climate-change velocities based on gradients of  
126 isotherms alone (3, 24), climate analogue mapping allows to consider consolidated changes of multiple  
127 bioclimatic variables at the same time. For example, we here simultaneously consider changes in maximum  
128 growing-season temperatures, minimum winter temperatures and growing-season precipitation as one  
129 measure of the climate change velocity between the baseline survey and resurvey periods (**Fig. S2**). This is  
130 highly relevant because plants respond not only to warming temperatures but also to alterations in  
131 precipitation regimes. In this method, for all resurveyed vegetation plots, a grid search (at  $4\ km \times 4\ km$   
132 resolution) was performed to map all raster cells within the study area in which the climatic conditions in  
133 the resurvey period are similar (i.e., show no statistical difference) to a given plot's climate during the  
134 baseline period (i.e., 'analogue climate conditions'). For each plot, we then located the position of the  
135 nearest raster cell with analogue climatic conditions to calculate the velocity and geographic direction of  
136 climate change over time. Identical to the centroid shifts, the climate change velocity for each plot was  
137 expressed as the absolute shift velocity ( $km\ year^{-1}$ ), as well as the projected south-north ( $km\ north\ year^{-1}$ )  
138 and west-east ( $km\ east\ year^{-1}$ ) velocity. The directionality of climate analogue shifts was tested using  
139 Rayleigh's  $r$  coefficient as described above.

140 Centroid shifts across the 266 understory plant species varied between  $0.006\ km\ year^{-1}$  (*Symphytum*  
141 *cordatum*) to  $18.27\ km\ year^{-1}$  (*Abies alba* seedlings), and occurred at a mean rate of  $3.56$  (5% – 95%  
142 quantile:  $0.39$  –  $9.80$ )  $km\ year^{-1}$  (**Fig. 2A, Data S1**). Surprisingly, two-thirds of the studied plant species  
143 showed directional shifts along the west-east axis (Rayleigh's  $r = 0.23$ ;  $df = 265$ ;  $p < 0.05$ ). Most of these

144 shifts were westward (39% of species), but we also noted many eastward shifts (23%). Southward shifts  
145 (23%) were more frequent than northward shifts (15%). Westward range centroid shifts were thus 2.6 times  
146 more likely than the northward range shifts expected in response to climate change. The average south-  
147 north rate of centroid shifts was slow but significantly equatorward (-0.63 [-4.30 – 2.89] km north year<sup>-1</sup>;  
148 one-sample t-test:  $t = -4.36$ ,  $df = 265$ ,  $p < .001$ ), while the rate of west-east shifts was 1.8 times faster and  
149 significantly westward (-1.17 [-6.95 – 4.17] km east year<sup>-1</sup>; one-sample t-test:  $t = -4.90$ ,  $df = 265$ ,  $p < .001$ ).  
150 The observed rates of centroid shifts towards each cardinal direction were minimum 62% (southward shifts)  
151 and maximum 70% (eastward shifts) faster than expected by chance as confirmed by a null-model approach  
152 (**Fig. S5**).

153 The climate significantly changed over the course of the study period in 2,949 of the 2,954 resurveyed  
154 vegetation plots (99.8%) based on climate analogue mapping. Maximum growing-season temperatures  
155 increased by an average of 1.59 [1.15 – 2.21] °C. Climate change took place at an average absolute velocity  
156 of 0.66 (0.07 – 1.67) km year<sup>-1</sup> (**Fig. 2B**). Unsurprisingly, the dominant geographic direction of climate  
157 change was north (40% of the plots; Rayleigh's  $r = 0.29$ ;  $df = 2,948$ ;  $p < 0.05$ ). The south-north velocity of  
158 climate change was also significantly northward (0.24 [-0.72 – 1.94] km north year<sup>-1</sup>; one-sample t-test:  $t =$   
159 18.15,  $df = 2,948$ ,  $p < .001$ ). The west-east climate change velocity was marginal but significantly eastward  
160 (0.06 [-0.92 – 0.72] km east year<sup>-1</sup>; one-sample t-test:  $t = 5.55$ ,  $df = 2,948$ ,  $p < .001$ ) and thus opposite to  
161 the most common cardinal direction of centroid shifts of European forest plants.

162 Neither the geographic direction nor the velocity of climate change was reflected in the species' centroid  
163 shifts, hinting towards the importance of other environmental changes. Two prominent alternative drivers  
164 of forest plant community changes are elevated atmospheric inputs of nitrogen and forest canopy cover  
165 changes (16, 25–28), with eutrophying effects of nitrogen complicated by recovery dynamics from past  
166 acidification caused by the combined deposition of nitrogen and sulphur compounds (29, 30). These drivers  
167 show spatial patterns not confounded with the velocity of climate change (across all plots, pairwise  
168 Spearman correlations between the south-north velocity of climate change *versus* the rates of nitrogen  
169 deposition and forest canopy cover changes were only 0.04 and 0.01, respectively).

170 To better understand the potential drivers associated with the reported changes in the geographical  
171 distribution of species, we related the rates of centroid shifts to the average rate of nitrogen deposition  
172 between the baseline survey and resurvey ( $kg N ha^{-1} year^{-1}$ ) extracted from atmospheric deposition maps at  
173 0.1° resolution (*c.* 8 km × 8 km within the study area) (**Fig. 1A**), and to the observed rate of forest canopy  
174 cover change at each site ( $% canopy cover increase year^{-1}$ ), while also accounting for the velocity of climate  
175 change (the absolute, south-north and west-east velocity) in a linear mixed-effects modeling framework.  
176 We furthermore tested for the potential confounding effect of past acidifying deposition, considering the

177 known adverse effects on European forest plant communities (31). The acidifying deposition rate, however,  
178 was highly correlated to the rate of nitrogen deposition over the course of the study due to partially shared  
179 emission sources (Spearman correlation: 0.87;  $n = 2,954$  plots), and their individual effects are therefore  
180 difficult to tease apart in an observational study. We calculated species-specific experienced rates of  
181 atmospheric (nitrogen and acidifying) deposition and forest canopy cover changes as the average rate across  
182 all plots where the species was observed, weighted by the species' original abundance in the baseline time  
183 period survey (**Fig. S6** for a data flow chart).

184 Model outputs show that the absolute rate of centroid shifts was weakly but exclusively linked to the rate  
185 of forest canopy change, with greater opening of the canopy enhancing centroid shifts (**Fig. 3**). The velocity  
186 of climate change was not associated to the rates of centroid shifts. In contrast, the rate of nitrogen  
187 deposition was significantly linked to the west-east rate of centroid shifts, with species that initially  
188 experienced a lower nitrogen deposition rate across their distributions showing faster westward shifts (**Fig.**  
189 **3A**). Variation partitioning revealed that the nitrogen deposition rate rather than the climate change velocity  
190 explained most of the variation in the species' centroid shifts, albeit the proportion of variation explained  
191 was small (**Figs. 3B, S7**). The estimated effects of past acidifying deposition on species centroid shifts were  
192 nearly identical to the effects of the spatially correlated nitrogen deposition rate (**Fig. S8**). We are therefore  
193 unable to distinguish with certainty whether centroid shifts were brought about by eutrophying rather than  
194 changes in acidifying deposition, or a combination of both. In either case, however, atmospheric deposition  
195 rates – and not the climate change velocities – were the superior predictors of westward species movements.

## 196 **Colonization and extinction centroids**

197 To shed light on the mechanisms driving centroid shifts, we decomposed centroid shifts into shifts attributed  
198 to the individual contribution of colonization and local extinction. For this analysis, we introduce the  
199 concept of colonization centroids (the centroid of plots newly colonized by a species, abundance-weighted  
200 by the percentage cover in the resurvey) and extinction centroids (the centroid of plots in which a species  
201 became extinct, abundance-weighted by the percentage cover in the baseline survey). Colonization and  
202 extinction centroids were expressed as the projected distance from the species' baseline centroid position  
203 in each geographic direction (*km north* and *km east*). From a biogeographical point of view, longer distances  
204 reflect that colonization or local extinction events took place farther away from the baseline centroid,  
205 suggesting that these processes occurred mostly in one preferred direction (schematically explained in **Fig.**  
206 **S1C**).

207 The average absolute distance of colonization centroids (202.20 [28.30 – 478.46] km;  $n$  species = 202) was  
208 larger than the average absolute distance of extinction centroids (82.22 [4.22 – 249.48] km;  $n$  species =

209 246; **Figs. 4, S9, S10**). Colonization centroids were also more isotropic across species (Rayleigh's  $r = 0.32$ ;  
210  $df = 201$ ;  $p < 0.05$ ) than extinction centroids (Rayleigh's  $r = 0.11$ ;  $df = 245$ ;  $p < 0.05$ ). This suggests that  
211 colonization events were happening more in one preferred direction and occurred further away from  
212 baseline range centroids (i.e., closer to range boundaries) compared to local extinctions.

213 Colonization along the west-east axis was most closely related to the nitrogen deposition rate (**Figs. S11,**  
214 **S12**). Because the observed dominant direction of species' colonization was westward (39% of the species  
215 colonized west, 21% east, 28% south and 12% north), colonization occurred more frequently for species  
216 that initially experienced a lower rate of nitrogen depositions across their distributions. This pattern is  
217 possibly associated to the westward colonization of nitrogen generalist species that can take advantage of  
218 eutrophic conditions such as observed in large parts of western Europe (**Figs. 1A, S13**). Indeed, linking the  
219 colonization centroids to each species' ecological indicator value for nitrogen niche width (with larger  
220 values indicating generalist species with a broader niche) (32) revealed that for nitrogen generalists in  
221 particular, those that initially occurred in areas with a lower rate of nitrogen deposition have taken  
222 advantage to move more westward (**Figs. 5, S14**). Nitrogen generalists that already occurred in areas with  
223 higher nitrogen deposition (western Europe, **Figs. 1A, S13**) tended to remain in place without necessarily  
224 moving westward. More specialist species, i.e. those with narrow niche widths for nitrogen and that often  
225 also have smaller range sizes (33), have shown lower colonization rates across temperate Europe, allowing  
226 generalist species to replace specialists (14). Also the decreasing levels of acidifying deposition (since the  
227 peak in the 1980s (34)) may have facilitated the recovery of species' ranges in formerly polluted regions  
228 (30). Using our observational data, we cannot fully disentangle these recovery effects following past  
229 acidification caused by both nitrogen and sulphur pollution from dynamics of eutrophication chiefly  
230 involving nitrogen deposition. However, eutrophication may be the most likely driver, because (i) we show  
231 that west-east colonization distances were statistically better linked to nitrogen deposition and the species'  
232 nitrogen niche width than to acidifying deposition and the species acidity niche width (**Fig. S15**); and (ii)  
233 the vast majority of the vegetation plots appear to be relatively well buffered against soil acidification (**Fig.**  
234 **S16**). Regardless of whether the driver of westward colonization chiefly involves eutrophying deposition  
235 or facilitated by the recovery from past acidification, forest plant species native to regions with lower  
236 deposition rates are more vulnerable to unanticipated range shifts in response to atmospheric pollution – a  
237 key finding for forest biodiversity conservation policy.

238 Local extinction events along the south-north axis were preferentially located southward relative to the  
239 species' baseline range centroid position, and thus closer to species' warm range limits (25% south *versus*  
240 13% north) (**Fig. 4**). This trend was significantly associated with climate change and a higher rate of  
241 nitrogen deposition (**Figs. S11, S12**). Local extinction events along the west-east axis, however, occurred

242 more often (28% east and 31% west). Eastward local extinctions occurred more commonly in species that  
243 experienced a higher rate of nitrogen deposition across their distribution. Such nitrogen-mediated local  
244 extinctions were amplified when forest canopies became more open. Velocities of climate change also  
245 interacted with the rate of forest canopy cover change, in that local extinctions due to climate change  
246 occurred more often in forests where the canopy cover decreased. This confirms the importance of tree  
247 canopies buffering the impacts of environmental changes (35).

248 Our findings suggest that atmospheric deposition and forest canopy cover dynamics interact to determine  
249 how forest plant species are shifting their ranges, and that these environmental changes induce shifts that  
250 can be independent from isotherm shifts. This contradicts the idea that species have shifted ranges mainly  
251 in response to warming air temperatures. Rather, other environmental changes, especially rates of  
252 atmospheric deposition and forest canopy cover dynamics, have likely induced unexpected westward range  
253 shifts in European forest plants. Although it remains unclear whether the effect of atmospheric deposition  
254 chiefly involves eutrophication or a recovery effect from past acidification due to both nitrogen and sulphur  
255 pollution, our findings point at nitrogen deposition as the most likely driver explaining the westward range  
256 shifts in European forest plants. Since the continued success of the United Nations air convention  
257 (CLRTAP) and the European Union Emissions Ceiling Directive (NECD) in reducing nitrogen and sulphur  
258 emission levels, prospective trends in climate change and atmospheric deposition are unlikely parallel, with  
259 climate change outpacing the effects of atmospheric deposition on future species' range shifts. Accurate  
260 and recent species range shift data will be key to adequately anticipate the respective impacts of climate  
261 change and atmospheric deposition on biodiversity and ecosystem functioning. It is already clear, however,  
262 that biodiversity redistribution patterns appear complex and are more likely driven by the interplay among  
263 several environmental changes than due to the exclusive effect of climate change alone.

264 **References:**

- 265 1. J. Lenoir, R. Bertrand, L. Comte, L. Bourgeaud, T. Hattab, J. Murienne, G. Grenouillet, Species better track  
266 climate warming in the oceans than on land. *Nat. Ecol. Evol.* **4**, 1044–1059 (2020).
- 267 2. I. Chen, J. K. Hill, R. Ohlemüller, D. B. Roy, C. D. Thomas, Rapid Range Shifts of Species of Climate  
268 Warming. *Science (80-. )*. **333**, 1024–1027 (2011).
- 269 3. M. T. Burrows, D. S. Schoeman, L. B. Buckley, P. Moore, E. S. Poloczanska, K. M. Brander, C. Brown, J. F.  
270 Bruno, C. M. Duarte, B. S. Halpern, J. Holding, C. V Kappel, W. Kiessling, M. I. O’Connor, J. M. Pandolfi,  
271 C. Parmesan, F. B. Schwing, W. J. Sydeman, A. J. Richardson, The Pace of Shifting Climate in Marine and  
272 Terrestrial Ecosystems. *Science (80-. )*. **334**, 652–656 (2011).
- 273 4. J. W. Williams, S. T. Jackson, Novel climates, no-analog communities, and ecological surprises. *Front. Ecol.*  
274 *Environ.* **5**, 475–782 (2007).
- 275 5. C. Parmesan, N. Ryrholm, C. Stefanescu, J. K. Hill, C. D. Thomas, H. Descimon, B. Huntley, L. Kaila, J.  
276 Kullberg, T. Tammaru, W. J. Tennent, J. A. Thomas, M. Warren, Poleward shifts in geographical ranges of  
277 butterfly species associated with regional warming. *Nature* **399**, 579–583 (1999).
- 278 6. J. Lenoir, P. A. Marquet, P. De Ruffray, H. Brisse, A Significant Upward Shift in Plant Species Optimum  
279 Elevation During the 20th Century. *Science (80-. )*. **320**, 1768–1772 (2008).
- 280 7. R. Virkkala, A. Lehikoinen, Patterns of climate-induced density shifts of species: poleward shifts faster in  
281 northern boreal birds than in southern birds. *Glob. Chang. Biol.* **20**, 2995–3003 (2014).
- 282 8. S. Dullinger, A. Gattlinger, W. Thuiller, D. Moser, N. E. Zimmermann, A. Guisan, W. Willner, C. Plutzer,  
283 M. Leitner, T. Mang, M. Caccianiga, T. Dirnböck, S. Ertl, A. Fischer, J. Lenoir, J. Svenning, A. Psomas, D.  
284 R. Schmatz, Extinction debt of high-mountain plants under twenty-first-century climate change. *Nat. Clim.*  
285 *Chang.* **2**, 6–9 (2012).
- 286 9. C. Parmesan, G. Yohe, A globally coherent fingerprint of climate change impacts across natural systems.  
287 *Nature* **421**, 37–42 (2003).
- 288 10. M. A. Rubenstein, S. R. Weiskopf, R. Bertrand, S. L. Carter, L. Comte, M. J. Eaton, C. G. Johnson, J. Lenoir,  
289 A. J. Lynch, B. W. Miller, T. L. Morelli, M. A. Rodriguez, A. Terando, L. M. Thompson, Climate change and  
290 the global redistribution of biodiversity: substantial variation in empirical support for expected range shifts.  
291 *Environ. Evid.* **12**, 1–21 (2023).
- 292 11. L. P. Shoo, S. E. Williams, J. Hero, Detecting climate change induced range shifts: Where and how should  
293 we be looking? *Austral Ecol.* **31**, 22–29 (2006).
- 294 12. J. D. Ash, T. J. Givnish, D. M. Waller, Tracking lags in historical plant species’ shifts in relation to regional  
295 climate change. *Glob. Chang. Biol.* **23**, 1305–1315 (2017).
- 296 13. T. L. Greaver, C. M. Clark, J. E. Compton, D. Vallano, A. F. Talhelm, C. P. Weaver, L. E. Band, J. S. Baron,  
297 E. A. Davidson, C. L. Tague, E. Felker-Quinn, J. A. Lynch, J. D. Herrick, L. Liu, C. L. Goodale, K. J. Novak,  
298 R. A. Haeuber, Key ecological responses to nitrogen are altered by climate change. *Nat. Clim. Chang.* **6**, 836–  
299 843 (2016).
- 300 14. I. R. Staude, D. M. Waller, M. Bernhardt-Römermann, A. D. Bjorkman, J. Brunet, P. De Frenne, R. Hédli, U.  
301 Jandt, J. Lenoir, F. Máliš, K. Verheyen, M. Wulf, H. M., Pereira, P. Vangansbeke, A. Ortman-Ajkai, R.  
302 Pielech, I. Berki, M. Chudomelová, G. Decocq, T. Dirnböck, T. Durak, T. Heinken, B. Jaroszewicz, M.  
303 Kopecký, M. Macek, M. Malicki, T. Naaf, T. A. Nagel, P. Petřík, K. Reczyńska, F. H. Schei, W. Schmidt, T.  
304 Standovár, K. Świerkosz, B. Teleki, H. Van Calster, O. Vild, L. Baeten, Replacements of small- by large-  
305 ranged species scale up to diversity loss in Europe’s temperate forest biome. *Nat. Ecol. Evol.* **4**, 802–808  
306 (2020).
- 307 15. C. Senf, R. Seidl, Mapping the forest disturbance regimes of Europe. *Nat. Sustain.* **4**, 63–70 (2021).

- 308 16. P. Sanczuk, K. De Pauw, E. De Lombaerde, M. Luoto, C. Meeussen, S. Govaert, T. Vanneste, L. Depauw, J.  
309 Brunet, S. A. O. Cousins, C. Gasperini, P. Hedwall, G. Iacopetti, J. Lenoir, J. Plue, F. Selvi, F. Spicher, J.  
310 Uria-diez, K. Verheyen, P. Vangansbeke, P. De Frenne, Microclimate and forest density drive plant population  
311 dynamics under climate change. *Nat. Clim. Chang.* **13**, 840–847 (2023).
- 312 17. S. M. Crimmins, S. Z. Dobrowski, J. A. Greenberg, J. T. Abatzoglou, A. R. Mynsberge, Changes in Climatic  
313 Water Balance Drive Downhill Shifts in Plant Species' Optimum Elevations. *Science (80-. )*. **331**, 324–327  
314 (2011).
- 315 18. D. Jacobsen, The dilemma of altitudinal shifts: caught between high temperature and low oxygen. *Front. Ecol.*  
316 *Environ.* **18**, 211–218 (2020).
- 317 19. J. Lenoir, J. Ge, A. Guisan, P. Vittoz, T. Wohlgemuth, N. E. Zimmermann, S. Dullinger, H. Pauli, W. Willner,  
318 J. Svenning, Going against the flow: potential mechanisms for unexpected downslope range shifts in a  
319 warming climate. *Ecography (Cop.)*. **33**, 295–303 (2010).
- 320 20. D. M. Olson, E. Dinerstein, E. D. Wikramanayake, N. D. Burgess, G. V. N. Powell, E. C. Underwood, J. A.  
321 D. Amico, I. Itoua, H. E. Strand, J. C. Morrison, J. Loucks, T. F. Allnutt, T. H. Ricketts, Y. Kura, J. F.  
322 Lamoreux, W. Wesley, P. Hedao, K. R. Kassem, Terrestrial Ecoregions of the World: A New Map of Life on  
323 Earth. *Bioscience* **51**, 933–938 (2001).
- 324 21. J. Vanderwal, H. T. Murphy, A. S. Kutt, G. C. Perkins, B. L. Bateman, J. J. Perry, A. E. Reside, Focus on  
325 poleward shifts in species' distribution underestimates the fingerprint of climate change. *Nat. Clim. Chang.* **2**,  
326 1–5 (2012).
- 327 22. M. C. Fitzpatrick, R. R. Dunn, Contemporary climatic analogs for 540 North American urban areas in the late  
328 21st century. *Nat. Commun.* **614**, 1–7 (2019).
- 329 23. J. W. Williams, S. T. Jackson, J. E. Kutzbach, Projected distributions of novel and disappearing climates by  
330 2100 AD. *PNAS* **104**, 5738–5742 (2007).
- 331 24. S. R. Loarie, P. B. Duffy, H. Hamilton, G. P. Asner, C. B. Field, D. D. Ackerly, The velocity of climate  
332 change. *Nature* **462**, 1052–1055 (2009).
- 333 25. P. De Frenne, B. J. Graae, F. Rodríguez-Sánchez, A. Kolb, O. Chabrierie, G. Decocq, H. De Kort, A. De  
334 Schrijver, M. Diekmann, O. Eriksson, R. Gruwez, M. Hermy, J. Lenoir, J. Plue, D. A. Coomes, K. Verheyen,  
335 Latitudinal gradients as natural laboratories to infer species' responses to temperature. *J. Ecol.* **101**, 784–795  
336 (2013).
- 337 26. J. Segar, H. M. Pereira, L. Baeten, M. Bernhardt-römermann, P. De Frenne, N. Fernández, F. S. Gilliam, J.  
338 Lenoir, A. Ortmann-ajkai, K. Verheyen, D. Waller, B. Teleki, J. Brunet, M. Chudomelová, G. Decocq, T.  
339 Dirnböck, R. Hédl, T. Heinken, B. Jaroszewicz, M. Kopecký, Martin Macek, F. Máliš, T. Naaf, A. Orczewska,  
340 K. Reczynska, W. Schmidt, J. Šebesta, A. Stachurska-Swakoń, T. Standovár, K. Swierkosz, O. Vild, M. Wulf,  
341 I. R. Staude, Divergent roles of herbivory in eutrophying forests. *Nat. Commun.* **13**, 1–10 (2022).
- 342 27. K. Verheyen, L. Baeten, P. De Frenne, M. Bernhardt-ro, J. Cornelis, G. Decocq, H. Dierschke, O. Eriksson,  
343 T. Heinken, M. Hermy, P. Hommel, K. Kirby, G. Walther, M. Wulf, G. Verstraeten, Driving factors behind  
344 the eutrophication signal in understory plant communities of deciduous temperate forests. *J. Ecol.* **100**, 352–  
345 365 (2012).
- 346 28. P.-O. Hedwall, J. U.- Diez, J. Brunet, L. Gustafsson, A.-L. Axelsson, J. Strengbom, Interactions between local  
347 and global drivers determine long- term trends in boreal forest understory vegetation. *Glob. Ecol. Biogeogr.*  
348 **30**, 1765–1780 (2021).
- 349 29. N. Duarte, L. H. Pardo, M. J. Robin-Abbott, Susceptibility of Forests in the Northeastern USA to Nitrogen  
350 and Sulfur Deposition: Critical Load Exceedance and Forest Health. *Water, Air Soil Pollut.*, 1–21 (2013).
- 351 30. E. Tipping, J. A. C. Davies, P. A. Henrys, S. G. Jarvis, S. M. Smart, Long-term effects of atmospheric  
352 deposition on British plant species. *Environ. Pollut.* **281**, 117017 (2021).

- 353 31. G. Riofrio-Dillon, R. Bertrand, J.-C. Gégout, Toward a recovery time: forest herbs insight related to  
354 anthropogenic acidification. *Glob. Chang. Biol.* **18**, 3383–3394 (2012).
- 355 32. J. Dengler, F. Jansen, O. Chusova, E. Hüllbusch, M. P. Nobis, K. Van Meerbeek, I. Axmanová, H. H. Bruun,  
356 M. Chytrý, R. Guarino, G. Karrer, K. Moeys, T. Raus, M. J. Steinbauer, Y. Didukh, M. Diekmann, T. Englisch,  
357 E. Fernández-pascual, P. Julve, G. Nakhutsrishvili, W. A. Ozinga, E. Ruprecht, U. Šilc, J.-P. Theurillat, F.  
358 Gillet, Ecological Indicator Values for Europe (EIVE) 1.0. *Veg. Classif. Surv.* **4**, 7–29 (2023).
- 359 33. S. Kambach, J. Lenoir, G. Decocq, E. Welk, G. Seidler, S. Dullinger, J. Gégout, A. Guisan, H. Pauli, J.  
360 Svenning, P. Vittoz, T. Wohlgemuth, N. E. Zimmermann, H. Bruelheide, Of niches and distributions: range  
361 size increases with niche breadth both globally and regionally but regional estimates poorly relate to global  
362 estimates. *Ecography (Cop.)*. **42**, 467–477 (2019).
- 363 34. P. Grennfelt, A. Engleryd, M. Forsius, Ø. Hov, H. Rodhe, E. Cowling, Acid rain and air pollution: 50 years  
364 of progress in environmental science and policy. *Ambio* **49**, 849–864 (2020).
- 365 35. P. De Frenne, Novel light regimes in European forests. *Nat. Ecol. Evol.* **8**, 196–202 (2024).
- 366 36. J. T. Abatzoglou, S. Z. Dobrowski, S. A. Parks, K. C. Hegewisch, TerraClimate, a high-resolution global  
367 dataset of monthly climate and climatic water balance from 1958 – 2015. *Sci. Data* **5**, 1–12 (2018).
- 368 37. EMEP, *EMEP Status Report 1/2023 “Transboundary Particulate Matter, Photo-Oxidants, Acidifying and*  
369 *Eutrophying Components”* (2023).
- 370 38. European Environment Agency. <https://www.eea.europa.eu/en/datahub/datahubitem-view/>.
- 371 39. P. Sanczuk, K. Verheyen, J. Lenoir, F. Zellweger, J. Lembrechts, R.-S. Francisco, L. Baeten, M. Bernhardt-  
372 Römermann, K. De Pauw, P. Vangansbeke, M. Perring, I. Berki, A. Bjorkmann, J. Brunet, M. Chudomelová,  
373 E. De Lombaerde, G. Decocq, T. Dirnböck, T. Durak, C. Greiser, R. Hédl, T. Heinken, U. Jandt, B.  
374 Jaroszewicz, M. Kopecky, D. Landuyt, M. Macek, F. Máliš, T. Naaf, T. Nagel, P. Petřík, K. Reczynska, W.  
375 Schmidt, T. Standovar, I. Staude, K. Świerkosz, B. Teleki, T. Vanneste, O. Vild, D. Waller, P. De Frenne,  
376 Data and Code associated with original research article: Nitrogen deposition mediates westward range shifts  
377 in European forest plants [Dataset]. *Dryad*, doi: doi.org/10.5061/dryad.4b8gthtmt (2024).
- 378 40. P. De Frenne, F. Rodriguez-Sanchez, D. A. Coomes, L. Baeten, G. Verstraeten, M. Vellend, M. Bernhardt-  
379 Romermann, C. D. Brown, J. Brunet, J. Cornelis, G. M. Decocq, H. Dierschke, O. Eriksson, F. S. Gilliam, R.  
380 Hedl, T. Heinken, M. Hermy, P. Hommel, M. A. Jenkins, D. L. Kelly, K. J. Kirby, F. J. G. Mitchell, T. Naaf,  
381 M. Newman, G. Peterken, P. Petrik, J. Schultz, G. Sonnier, H. Van Calster, D. M. Waller, G.-R. Walther, P.  
382 S. White, K. D. Woods, M. Wulf, B. J. Graae, K. Verheyen, Microclimate moderates plant responses to  
383 macroclimate warming. *PNAS* **110**, 18561–18565 (2013).
- 384 41. F. Zellweger, P. De Frenne, J. Lenoir, P. Vangansbeke, K. Verheyen, L. Baeten, R. Hédl, I. Berki, J. Brunet,  
385 H. Van Calster, M. Chudomelová, G. Decocq, T. Dirnböck, T. Durak, T. Heinken, B. Jaroszewicz, M.  
386 Kepecky, F. Máliš, M. Macek, M. Malicki, T. Naaf, T. A. Nagel, A. Ortmann-ajkai, P. Petrik, R. Pielech, K.  
387 Reczyn, W. Schmidt, R. Pielech, K. Reczynska, O. Vild, M. Wulf, D. Coomes, Forest microclimate dynamics  
388 drive plant responses to warming. *Science (80-. )*. **368**, 772–775 (2020).
- 389 42. S. A. Chamberlain, E. Szöcs, taxize: taxonomic search and retrieval in R. *F1000Research* **2**, 1–26 (2013).
- 390 43. J. Lenoir, J. Svenning, Climate-related range shifts – a global multidimensional synthesis and new research  
391 directions. *Ecography (Cop.)*. **38**, 15–28 (2015).
- 392 44. D. D. Breshears, T. E. Huxman, H. D. Adams, C. B. Zou, J. E. Davison, Vegetation synchronously leans  
393 upslope as climate warms. *PNAS* **105**, 11591–11592 (2008).
- 394 45. Edzer Pebesma, Simple Features for R: Standardized Support for Spatial Vector Data. *R J.* **10**, 439–446  
395 (2018).
- 396 46. R. J. Hijmans, geosphere: Spherical trigonometry. Retrieved from [https://cran.r-](https://cran.r-project.org/package=geosphere)  
397 [project.org/package=geosphere](https://cran.r-project.org/package=geosphere). (2017).

- 398 47. R. J. Hijmans, J. Van Etten, raster: Geographic analysis and modeling with raster data. R package version 2.0-  
399 12. doi: <http://cran.r-project.org/package=raster> (2012).
- 400 48. Microsoft, S. Weston, foreach: Provides Foreach Looping Construct. R package version 1.5.1. (2020).  
401 <https://cran.r-project.org/package=foreach>.
- 402 49. Microsoft, S. Weston, doParallel: Foreach Parallel Adaptor for the “parallel” Package. R package version  
403 1.0.16. (2020). <https://cran.r-project.org/package=doParallel>.
- 404 50. M. Tennekes, J. Nowosad, J. Gombin, S. Jeworutzki, K. Russell, R. Zijdeman, J. Clouse, R. Lovelace, J.  
405 Muenchow, tmap: Thematic Maps. *J. Stat. Softw.* **84**, 1–39 (2018).
- 406 51. C. Duprè, C. Stevens, T. Ranke, A. Bleekers, C. Pepler-Lisbach, D. Gowing, N. Dise, E. Dorland, R.  
407 Bobbink, M. Diekmann, Changes in species richness and composition in European acidic grasslands over the  
408 past 70 years: the contribution of cumulative atmospheric nitrogen deposition. *Glob. Chang. Biol.* **16**, 344–  
409 357 (2010).
- 410 52. D. Nieto-lugilde, J. Lenoir, S. Abdulhak, D. Aeschmann, S. Dullinger, J. Gégout, A. Guisan, H. Pauli, J.  
411 Renaud, J. Theurillat, W. Thuiller, J. Van Es, P. Vittoz, W. Willner, T. Wohlgemuth, N. E. Zimmermann, J.  
412 Svenning, Tree cover at fine and coarse spatial grains interacts with shade tolerance to shape plant species  
413 distributions across the Alps. *Ecography (Cop.)*. **38**, 578–589 (2015).
- 414 53. D. Bates, M. Mächler, B. M. Bolker, S. C. Walker, Fitting Linear Mixed-Effects Models Using lme4. *J. Stat.*  
415 *Softw.* **67**, 1–29 (2015).
- 416 54. C. F. Dormann, J. Elith, S. Bacher, C. Buchmann, G. Carl, G. Carr, J. R. Garc, B. Gruber, B. Lafourcade, P.  
417 J. Leit, M. Tamara, C. Mcclean, P. E. Osborne, B. S. Der, A. K. Skidmore, D. Zurell, S. Lautenbach,  
418 Collinearity: a review of methods to deal with it and a simulation study evaluating their performance.  
419 *Ecography (Cop.)*. **27**, 27–46 (2013).
- 420 55. K. Barton, MuMIn: Multi-Model Inference. (2017).
- 421 56. S. Nakagawa, H. Schielzeth, A general and simple method for obtaining R<sup>2</sup> from generalized linear mixed-  
422 effects models. *Methods Ecol. Evol.* **4**, 133–142 (2013).
- 423 57. R Core Team, *A Language and Environment for Statistical Computing*. R Foundation for Statistical  
424 Computing (Vienna, Austria, 2021).
- 425 58. B. Wen, H. Blondeel, L. Baeten, M. P. Perring, L. Depauw, S. L. Maes, L. De Keersmaeker, H. Van Calster,  
426 M. Wulf, T. Naaf, K. Kirby, M. Bernhardt-Römermann, T. Dirnböck, F. Máliš, M. Kopecký, O. Vild, M.  
427 Macek, R. Hédli, M. Chudomelová, J. Lenoir, J. Brunet, T. A. Nagel, K. Verheyen, D. Landuyt, Predicting  
428 trajectories of temperate forest understorey vegetation responses to global change. *For. Ecol. Manage.* **566**  
429 (2024).
- 430 59. B. Ulrich, “An ecosystem approach to soil acidification” in Ulrich B., Sumner M.E. (Eds). *Soil Acidity*.  
431 (Springer US, New York, 1991), pp. 28–79.

432

### 433 **Acknowledgements**

434 This paper is an outcome of the sREplot working group supported by sDiv, the Synthesis Centre of the  
435 German Centre for Integrative Biodiversity Research (iDiv) Halle-Jena-Leipzig (DFG FZT 118). **Funding:**  
436 PS, PDF, and PV received funding from the European Research Council (ERC) under the European Union's  
437 Horizon 2020 research and innovation programme (ERC Starting Grant FORMICA 757833) and Ghent  
438 University grant BOF23/GOA/019. FZ received funding from the Swiss National Science Foundation  
439 (project 193645). JLL received funding from the Flemish Research Organization (FWO, OZ7828, OZ7916  
440 and OZ7792). KDP received funding from the Flemish Research Organization (FWO, ASP035-19 De  
441 Pauw). IB was supported via grant EFOP-3.6.1.-16-2016-00018. AB received funding from the Knut and  
442 Alice Wallenberg Foundation (WAF KAW 2019.0202) and the Swedish Foundation for Strategic Research  
443 (FFL21-0194). MC was supported by the postdoctoral fellowship L200052302 of the Czech Academy of  
444 Sciences, grant 21-11487S by the Czech Science Foundation. MK, RH, MC, OV and MM were supported  
445 by the Czech Academy of Sciences (RVO 67985939). TD received funding from the eLTER PLUS project  
446 of the European Union Horizon 2020 (INFRAIA-01-2018-2019). CG received funding from FORMAS  
447 [project 2021-01993]. RH was supported by the Czech Science Foundation project 21-11487S. FM was  
448 supported by the project APVV-19-0319. PP was supported by the long-term development project of the  
449 Czech Academy of Sciences (RVO 67985939). FRS was supported by VI PPIT – US. **Author**  
450 **contributions:** PS and PDF conceived the ideas and designed the methodology, and with contributions of  
451 JL, JLL and FR; all authors collected data; PS analysed data in collaboration with PDF; PS led the writing  
452 of the manuscript in collaboration with PDF, and with significant contributions of KV, JL, FZ, JLL, FR,  
453 LB, MBR, KDP, PV and MPP. All authors contributed critically to the draft and gave final approval for  
454 publication. **Competing interests:** None of the authors have a conflict of interest. **Data and materials**  
455 **availability:** Raw macroclimate data can be accessed via the TerraClimate database (36). Historical  
456 nitrogen and sulphur deposition data can be accessed via the EMEP/CEIP 2023 Present state of emission  
457 data-base (37). Shapefile of biogeographical regions are provided by the European Environment Agency  
458 (38). Species' ecological indicator values of nitrogen niche width are provided by Dengler et al. (2023)  
459 (32). Raw data on species centroid shifts, environmental change data, and R scripts to reproduce the  
460 methods, analyses and source code of all figures are available [on Dryad \(39\)](#).

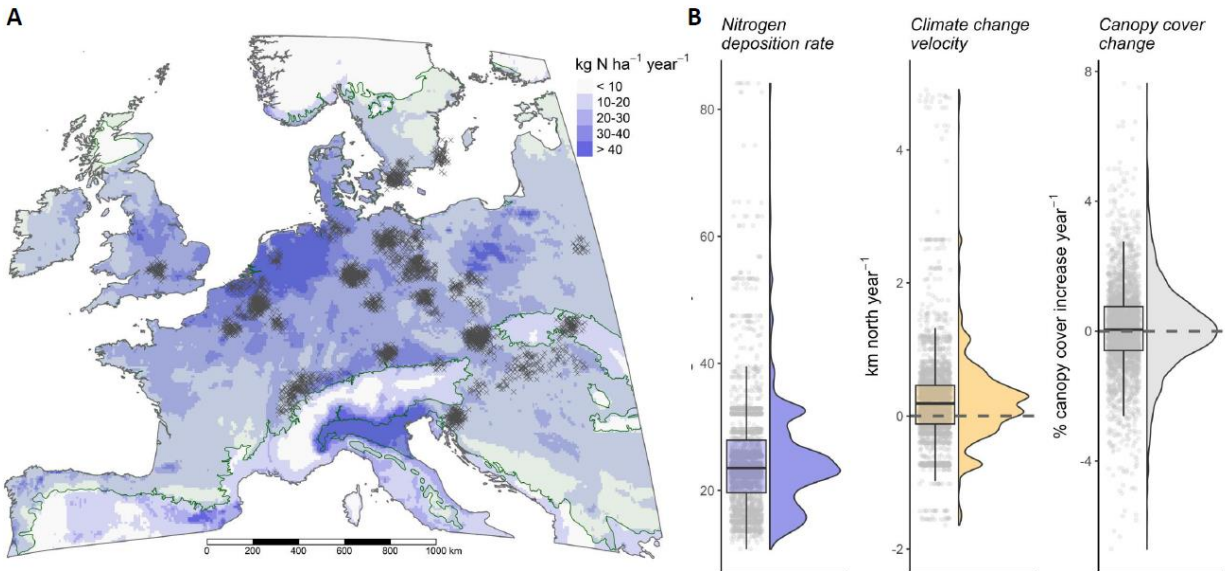
461

### 462 **Supplementary Materials**

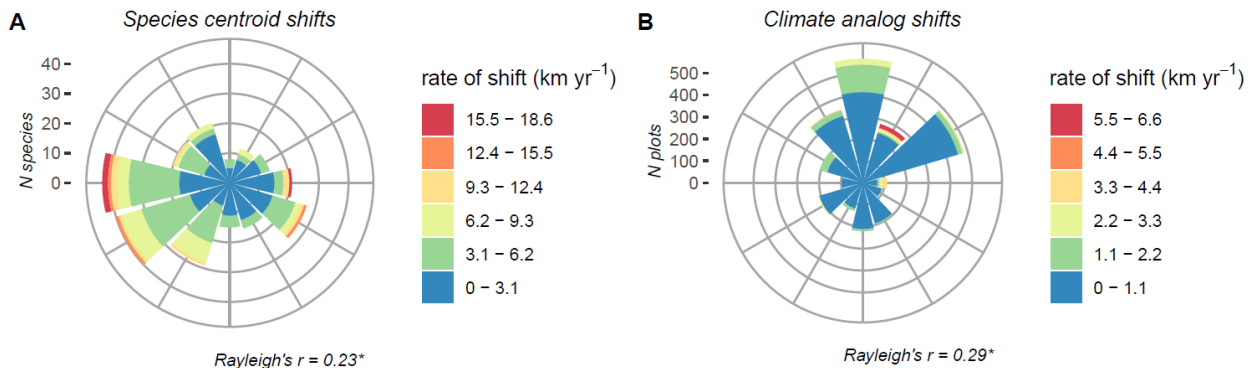
463           Methods

464           Figs. S1 to S16

465           Data S1

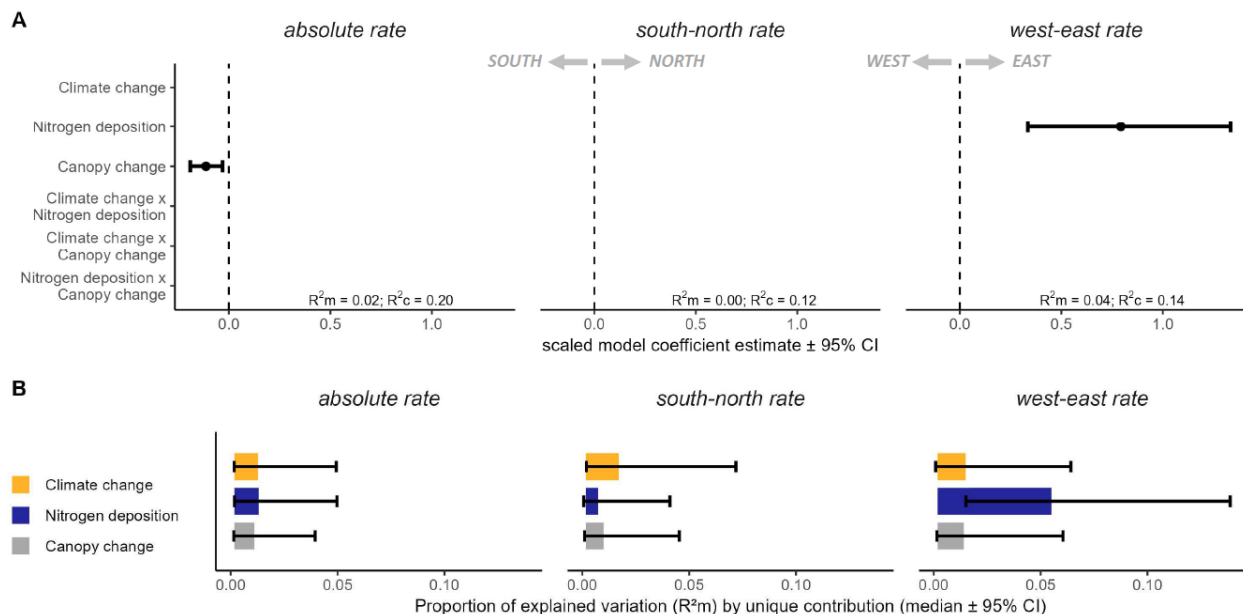


467  
 468 **Figure 1 | Spatial and environmental gradients of the study.** (A) Map of modelled nitrogen (N)  
 469 deposition rate (sum of oxidized and reduced wet and dry deposition expressed in  $\text{kg N ha}^{-1} \text{ year}^{-1}$ ; dry  
 470 deposition accounted for deciduous forest surface) at  $0.1^\circ$  resolution for the reference year 2000, and  
 471 distribution of the 2,954 resurveyed vegetation plots (grey crosses, spatially jittered for clarity) across the  
 472 European temperate forest biome (shaded green background) (20). (B) Observed environmental variation  
 473 across the 2,954 vegetation plots (grey dots) of three key drivers of forest biodiversity over the course of  
 474 the study period investigated here: nitrogen deposition rate (total of oxidized and reduced wet and dry N),  
 475 climate-change velocity (realized changes of both temperature and precipitation, expressed in  $\text{km north year}^{-1}$ )  
 476 and the rate of canopy cover change (average annual rate; expressed in  $\% \text{ canopy cover increase year}^{-1}$ ).  
 477 In all boxplots, we present the median (horizontal line), 1<sup>st</sup> and 3<sup>rd</sup> quantile (lower and upper hinges),  
 478 and 1.5 times the inter-quartile-range (whiskers). Half violin plots represent the density distributions of the  
 479 environmental change values. The grey dashed lines represent no changes (not shown for nitrogen  
 480 deposition rates). Negative values in the case of climate and canopy cover change indicate southward  
 481 velocities and canopy opening, respectively.

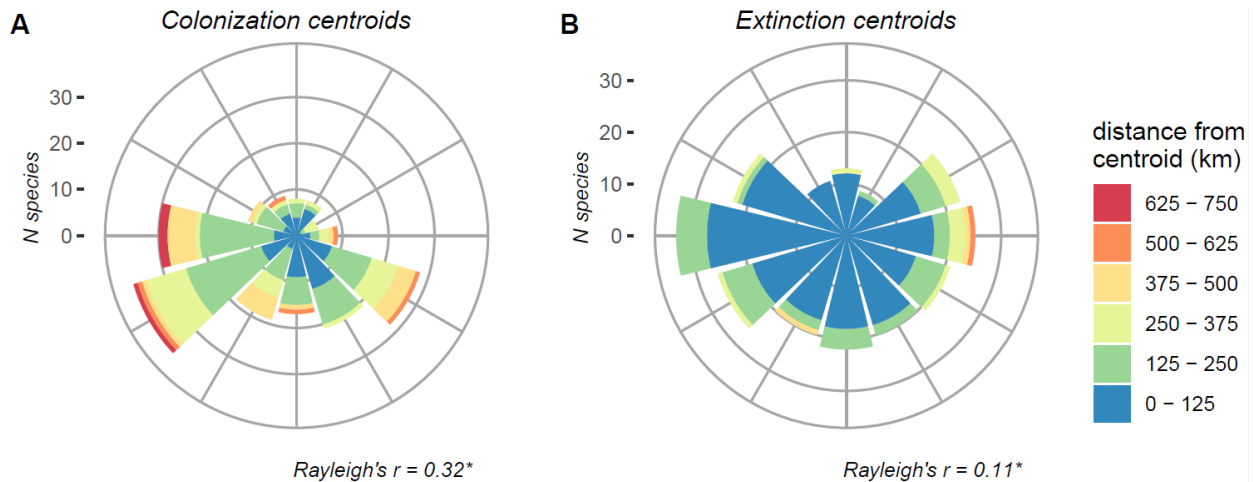


482  
 483 **Figure 2 | Rate and geographic direction of species centroid shifts and climate analogue shifts.** (A)  
 484 Rate and geographic direction of species range centroid shifts ( $n \text{ species} = 266$ ). (B) Velocity and  
 485 geographic direction of climate analogue shifts ( $n \text{ plots} = 2,954$ ). In all graphs, the Rayleigh's  $r$  statistic  
 486 represents a test of uniformity that compares the bearings of shifts to a uniform circular distribution (null  
 487 hypothesis). Larger values indicate more directional shifts. Asterisk (\*) indicates significant deviations

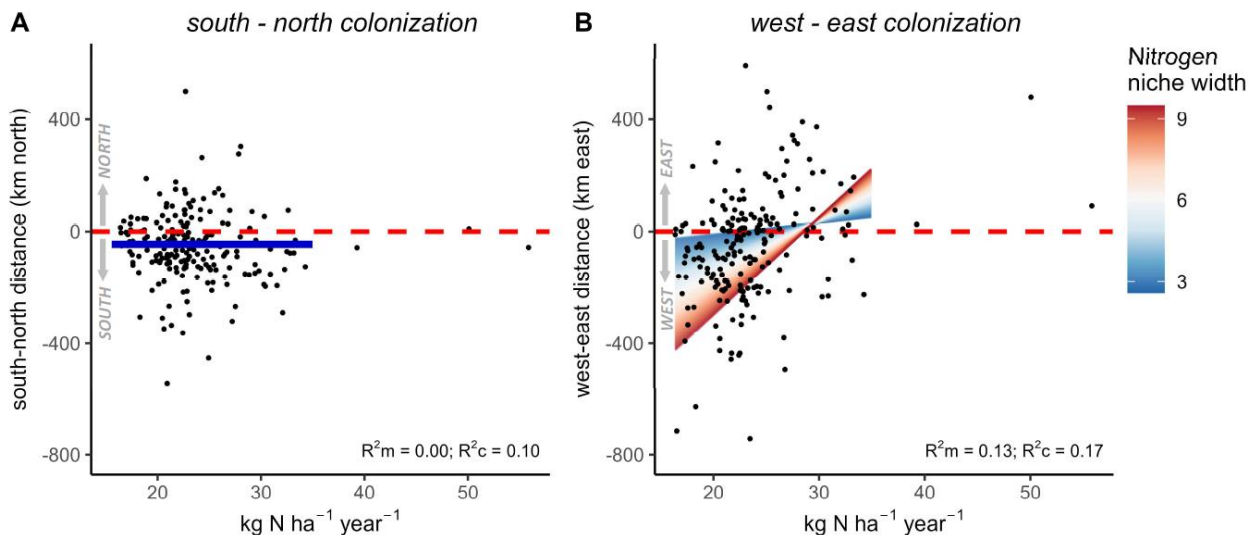
488 from the null hypothesis ( $p < 0.05$ ). See Figs. S3, S4 for results of the analyses including rare species and  
 489 per biogeographic region.



490  
 491 **Figure 3 | Effects of environmental changes on centroid shifts based on the most parsimonious model.**  
 492 (A) Results of the mixed-effects models ( $n$  species = 266) indicating coefficient estimates and 95%  
 493 confidence intervals (CI) of the effects of the velocity of climate change ( $km\ year^{-1}$ ,  $km\ north\ year^{-1}$ ,  $km$   
 494  $east\ year^{-1}$ ), average nitrogen deposition rate between the baseline survey and resurvey ( $kg\ N\ ha^{-1}\ year^{-1}$ ),  
 495 and rate of canopy change ( $\% cover\ increase\ year^{-1}$ ), as well as all pairwise interactions (indicated by ‘x’)  
 496 on the absolute rate of centroid shifts ( $km\ year^{-1}$ ) and the south-north rate ( $km\ north\ year^{-1}$ ; negative values  
 497 indicate southward shifts) and west-east rate ( $km\ east\ year^{-1}$ ; negative values indicate westward shifts)  
 498 extracted from the most parsimonious model structure (empty rows were not included in the final selected  
 499 model). All the predictor variables were  $z$ -transformed to increase comparability. Rates of canopy opening  
 500 (negative values of canopy change) are associated with greater absolute rates of centroid shifts. The west-  
 501 east rate was exclusively linked to nitrogen deposition, with faster westward shifts in species with lower  
 502 rates of nitrogen deposition across their distributions. Model fit is presented as the proportion of variation  
 503 explained by the fixed effect (marginal  $R^2$ ,  $R^2_m$ ) and the proportion of variation explained by the fixed and  
 504 random effects (conditional  $R^2$ ,  $R^2_c$ ). Models accounted for plant growth form as random intercept (five  
 505 levels: forbs, graminoids, pteridophytes, shrubs and trees). (B) Results of the variation partitioning analyses  
 506 representing the individual contribution of each environmental predictor. Bar plots are proportional to the  
 507 variation explained by the unique contribution of each fixed effect (expressed as  $R^2_m$ ). In all graphs,  
 508 estimates and error bars represent the median value and 2.5 – 97.5 percentiles across 1,000 bootstrap  
 509 samples. See **Fig. S7** for results on the analyses that also included rare species and **Fig. S8** for a direct  
 510 comparison with the estimated effects of acidifying deposition.



511  
 512 **Figure 4 | Distance and geographic direction of colonization and extinction centroids.** (A) Distance  
 513 and geographic direction of colonization centroids ( $n$  species = 202). (B) Distance and geographic direction  
 514 of extinction centroids ( $n$  = 246). Longer distances reflect that colonization or local extinction are happening  
 515 in one preferred direction relative to the baseline centroid. Rayleigh's  $r$  statistic represents a test of  
 516 uniformity that compares the bearings of shifts to a uniform circular distribution (null hypothesis). Larger  
 517 values indicate more directed shifts. Asterisk (\*) indicates significant deviations from the null hypothesis  
 518 ( $p < 0.05$ ). Results of the analyses that also included rare species are presented in **Fig. S9**. Results for each  
 519 biogeographic region are presented in **Fig. S10**.



520  
 521 **Figure 5 | Effects of nitrogen deposition rates and species nitrogen niche width on colonization**  
 522 **centroids in the most parsimonious models.** Results of the mixed-effects model testing for the interaction  
 523 effect between the average nitrogen deposition rate between the baseline survey and resurvey across each  
 524 species' distribution ( $\text{kg N ha}^{-1} \text{ year}^{-1}$ ) and species' ecological indicator values for nitrogen niche width (an  
 525 index integrating the intra- and inter-regional variability in the nitrogen niche, with higher values indicating  
 526 more generalist species and smaller values specialist species) on the south-north and west-east colonization  
 527 centroids. Negative distances indicate southward (A) or westward colonization (B). Interaction effects  
 528 between species nitrogen niche width and the average nitrogen deposition rate between the baseline survey  
 529 and resurvey across each species' distribution are plotted along the color gradient. Model predictions were  
 530 plotted to a maximum of  $35 \text{ kg N ha}^{-1} \text{ year}^{-1}$  to avoid extrapolation uncertainty for deposition values where  
 531 observations were scarce. Modelling results without outlier data ( $n = 3$  data points) are provided in **Fig.**  
 532 **S13**. The most parsimonious model of south-north colonization was an intercept-only model (blue solid

533 line). Westward colonization depended on species nitrogen niche width. Nitrogen generalists that initially  
534 occurred in areas with lower rates of nitrogen deposition moved more westward. Colonization in the more  
535 specialist species was generally suppressed, irrespective of the nitrogen deposition rate. In all plots, the red  
536 dashed line represents the zero-line.

537

538

539

## Supplementary Materials for

540

### 541 **Unexpected westward range shifts in European forest plants links to nitrogen** 542 **deposition**

543 Pieter Sanczuk<sup>1\*</sup>, Kris Verheyen<sup>1</sup>, Jonathan Lenoir<sup>2</sup>, Florian Zellweger<sup>3</sup>, Jonas J. Lembrechts<sup>4</sup>, Francisco  
544 Rodriguez-Sanchez<sup>5</sup>, Lander Baeten<sup>1</sup>, Markus Bernhardt-Römermann<sup>6,7</sup>, Karen De Pauw<sup>1</sup>, Pieter  
545 Vangansbeke<sup>1</sup>, Michael P. Perring<sup>8,9</sup>, Imre Berki<sup>10</sup>, Anne Bjorkman<sup>11,12</sup>, Jörg Brunet<sup>13</sup>, Markéta  
546 Chudomelová<sup>14</sup>, Emiel De Lombaerde<sup>14</sup>, Guillaume Decocq<sup>2</sup>, Thomas Dirnböck<sup>15</sup>, Tomasz Durak<sup>16</sup>,  
547 Caroline Greiser<sup>17,18</sup>, Radim Hédli<sup>14,19</sup>, Thilo Heinken<sup>20</sup>, Ute Jandt<sup>21,22</sup>, Bogdan Jaroszewicz<sup>23</sup>, Martin  
548 Kopecký<sup>24,25</sup>, Dries Landuyt<sup>1</sup>, Martin Macek<sup>24</sup>, František Máliš<sup>26,27</sup>, Tobias Naaf<sup>28</sup>, Thomas A. Nagel<sup>29</sup>,  
549 Petr Petřík<sup>30,31</sup>, Kamila Reczyńska<sup>32</sup>, Wolfgang Schmidt<sup>33</sup>, Tibor Standovár<sup>34</sup>, Ingmar Staude<sup>22,35</sup>,  
550 Krzysztof Świerkosz<sup>36</sup>, Balázs Teleki<sup>37</sup>, Thomas Vanneste<sup>1</sup>, Ondrej Vild<sup>14</sup>, Donald Waller<sup>38</sup>, Pieter De  
551 Frenne<sup>1</sup>

552 \*corresponding author : Pieter Sanczuk ; [Pieter.Sanczuk@UGent.be](mailto:Pieter.Sanczuk@UGent.be)

553

#### 554 **The PDF file includes:**

555 Methods

556 Figs. S1 to S16

557 Data S1

558

## 559 **Methods**

### 560 1. Study area and vegetation data

561 We compiled a database including 2,954 permanent and semi-permanent vegetation plots distributed in  
562 mature forest stands across five biogeographic regions (Atlantic [ $n$  plots = 322], Alpine [266], Boreal [21],  
563 Continental [2049] and Pannonian [296]) (**Fig. 1**; [www.forestREplot.ugent.be](http://www.forestREplot.ugent.be)) (40, 41). Community  
564 composition data were derived from baseline surveys recorded between 1933 and 1994 and paired resurveys  
565 carried out after the baseline surveys between 1987 and 2017 (median [min – max] inter-survey interval:  
566 39 [13 – 67] years). All plots were located in ancient (such that they have not been cleared for any other  
567 land use since at least the 18<sup>th</sup> century) mature forest stands and excluded heavily managed plantations.  
568 Vegetation plots did not experience major disturbances between the baseline surveys and the resurveys  
569 (e.g., no replanting or clearcutting). All plots were permanently marked (i.e., physical mark permanently  
570 visible in the field) or quasi-permanent. Plot sizes for botanical surveys ranged between 25 and 1300 m<sup>2</sup>.  
571 The presence and abundance (as the percentage ground cover, visually estimated) of all vascular plant  
572 species in the understorey (defined as all plants < 1.3 meter tall; thus including seedlings of tree and shrub  
573 species), was recorded in all plots. Plant taxonomy was standardized with the R package *taxize* (42).

574

### 575 2. Centroid shifts

#### 576 2.1. Rate (speed and direction) of range centroid shifts

577 Species centroid shifts are brought about by the combined effects of local colonization (a new arrival in the  
578 community of a given plot), changes in abundance, and local extinction, and these processes occur across  
579 the entire distribution of species (14, 43, 44). We quantified the rate of range shifts based on the actual  
580 change, over time, in the geographical coordinates of the range centroids, i.e., the abundance-weighted  
581 geometric center of a species' distribution across the vegetation plot network. In contrast to the more  
582 frequent quantification of range shifts from either the trailing or leading edges, analyzing centroid shifts  
583 allows us to obtain more robust estimates of the magnitude and geographic direction of complex  
584 distributional shifts (6, 11, 12, 21). This is important, since range shift estimates based on either leading or  
585 trailing edges can be affected by stochastic processes and low sample sizes that may blur the overall  
586 biogeographical trends (11).

587 Species' centroid shifts were quantified across all vegetation plots across the study area. To avoid bias  
588 attributed to rare species observed in only a few of the plots, we quantified range centroid shifts for all

589 species that occurred in more than 1% of the plots. Across the entire plot network, this resulted in a final  
590 set of 266 species. However, as a sensitivity analysis, range centroid shifts (and all downstream analyses)  
591 were also quantified for all species that occurred in more than 0.1% of the plots ( $N$  species = 596, for the  
592 entire plot network) (results in **Figs. S3, S7**). Centroid shifts for each separately biogeographic region  
593 (defined by the European Environment Agency; [www.eea.europa.eu](http://www.eea.europa.eu)) were also quantified by running the  
594 analyses on the subset of vegetation plots within each region (results in **Figs. S4, S9**). It is important to note  
595 here that the overall trends in centroid shifts across the entire study area are not directly comparable to the  
596 analyses for each biogeographic region separately, since likely disjunct shifts in different regions are  
597 averaged in the overall trends across the entire plot network.

598 We quantified the geographic displacement of centroids over time (schematically presented in **Fig. S1**) by  
599 means of the geographic distance and bearing (a circular variable expressed in decimal degrees ranging  
600 from  $0^\circ$  to  $360^\circ$ ) between species' centroid positions at the time of the baseline survey ( $t_1$ ) and at the time  
601 of the resurvey ( $t_2$ ) (12, 21). First, for each species, the mean latitude and longitude was calculated at  $t_1$  and  
602  $t_2$  weighted by the percentage cover (abundance-weighted) to locate the range centroids at the time of both  
603 surveys. Next, the geographic distance (minimal geodesic distance) between the centroids at  $t_1$  and  $t_2$  was  
604 quantified with the R package *sf* (45). The bearing was quantified as the geographical direction of travel  
605 along a rhumb line (so-called 'loxodrome', true course) between the centroids at  $t_1$  and  $t_2$  using the R  
606 package *geosphere* (46).

607 The distance and bearing of biotic centroid shifts were used to derive three response variables:

608 The absolute rate of centroid shifts ( $km\ year^{-1}$ ) was calculated as the geographic distance between the  
609 centroid at  $t_1$  and  $t_2$  (i.e. the length of the vector) divided by the average inter-survey interval in all plots  
610 where species  $sp_i$  was recorded.

611 The projected south-north and west-east rate ( $km\ north\ year^{-1}$  and  $km\ east\ year^{-1}$ ) of centroid shifts was  
612 calculated as the rate of centroid shift multiplied by the cosine (south-north rate) or the sine (west-east rate)  
613 of the geographic direction of shift.

614 The directionality (i.e., the angular dispersion of the bearings) of centroid shifts was quantified based on a  
615 Rayleigh's test of uniformity. In the Rayleigh's test, bearings of shifts are compared to a uniform circular  
616 distribution (i.e., the null hypotheses reflecting random shifts) to calculate Rayleigh's  $r$  statistic. This  
617 statistic represents the directionality of a set of vectors, ranging from zero (anisotropic distribution, meaning

618 random directional movements) to one (isotropic distribution; all vectors are centered to one single  
619 direction).

## 620 2.2. Distance of colonization and extinction centroids

621 To mechanistically unravel the processes at play in driving range centroid shifts, we decomposed centroid  
622 shifts of each species into shifts attributed to the effects of colonization (here, when a species is observed  
623 in a plot at  $t_2$  but not in  $t_1$ ), and shifts attributed to the effects of local extinction (when a species is observed  
624 in a plot at  $t_1$  but not in  $t_2$ ). For this analysis, we introduce the concept of colonization centroid- that is the  
625 centroid of newly colonized plots by a species (abundance-weighted by the percentage cover at  $t_2$ ) – and  
626 extinction centroid – that is the abundance-weighted centroid of plots where a species became locally  
627 extinct (abundance-weighted by the percentage cover at  $t_1$ ) (**Fig. S1**). Species-specific colonization and  
628 extinction centroids are expressed as the projected distance in each geographic direction (*km north* and *km*  
629 *east*) relative to the species' original centroid at  $t_1$ . The northward and eastward distances of the colonization  
630 and extinction centroids were calculated analogous to the rate of centroid shifts, but not accounting for the  
631 inter-survey interval. From a biogeographical point of view, longer distances reflect that colonization or  
632 local extinction events took place farther away from the baseline centroid, suggesting that these processes  
633 are happening in a preferred direction relative to the baseline centroid position (schematically explained in  
634 **Fig. S1C**). The directionality of the colonization and extinction centroids was quantified based on the  
635 Rayleigh's  $r$  statistic.

636 To avoid bias attributed to rare events of species colonization or local extinction in only a few of the plots,  
637 we quantified both centroid types for all species that colonized or went extinct in more than 1% of the plots.  
638 Across the entire plot network, this resulted in a final set of 202 species (colonization centroids) and 246  
639 species (extinction centroids). However, as a sensitivity analysis, both centroids (and all downstream  
640 analyses) were also quantified for all species that colonized or went locally extinct in more than 0.1% of  
641 the plots ( $n$  species = 527 and 542 for colonization and local extinction, respectively) (results in **Figs. S3,**  
642 **S7**).

## 643 2.3. Null model of random movements

644 To assess to what extent the centroid shifts are independent from noise attributed to, for instance, the spatial  
645 distribution of the vegetation plots, we applied a conservative null model approach as an additional  
646 sensitivity analysis. For each species, we calculated baseline and resurvey centroids from resampled (with  
647 replacement) plots in the vegetation data set. The baseline centroid was calculated based on a resample of

648 all plots where the species was observed in the baseline survey, with a sample size equal to the original data  
649 set in the baseline period. The resurvey centroid was calculated based on a sample of all plots where the  
650 species was observed in both the resurvey and baseline survey (thus, including also newly colonized plots  
651 and plots where the species went locally extinct), with a sample size equal to the original data set in the  
652 resurvey period. We thus assumed that the species could have moved randomly within its distribution (here,  
653 conservatively defined as all plots where the species was observed). The null model was iterated 1,000  
654 times for each species that was observed in >1% of the plots. Based on this sensitivity analysis, we conclude  
655 that the observed rate of centroid shifts was higher and the main directions less dispersed than would be  
656 expected at random owing to, for instance, the spatial distribution of the vegetation plots (i.e., shifts towards  
657 each cardinal direction were 62-70% faster than expected based on randomized shifts within each species'  
658 distribution; **Fig. S5**).

659

### 660 3. Environmental change variables

661 The absolute and projected velocities of species' centroid shifts and colonization and extinction centroids  
662 were linked to (i) the velocity of climate change (ii) nitrogen deposition rate and (iii) the rate of forest  
663 canopy cover change.

#### 664 3.1. The velocity of climate change

665 Spatially explicit climate change velocities were estimated by climate analogue mapping (4, 22), referring  
666 to the spatial change of climatic conditions (integrating both temperature and precipitation) between the  
667 baseline surveys and the resurveys. Climate analogue mapping is a statistical approach that maps all areas  
668 that have similar climatic conditions relative to a certain location's climate. Climate analogue mapping  
669 allowed us to quantify changes in the geographical distribution of climate over time, while also considering  
670 the geographic variation in climatic conditions at the landscape scale due to e.g., topoclimate. In contrast  
671 to the frequent calculation of climate change velocities based on thermal gradients and isotherms alone (3,  
672 24), climate analogue mapping allowed us to consider consolidated shifts of multiple bioclimatic variables,  
673 i.e. the maximum growing-season temperatures, mean minimum winter temperatures and total growing-  
674 season precipitation and represented the climatic norms over two ten-year periods (the baseline period  
675 [1958-1967] and resurvey period [2007-2016]; time interval of 49 years) (**Fig. S2**). Gridded monthly  
676 climate data were retrieved from the TerraClimate database (36) and analysed at 1/24<sup>th</sup> degree native  
677 resolution (approximately 4 km in the study area). We identified climate analogues for all 2,954 resurveyed

678 vegetation plots. For each plot, we performed a grid search at 4 km resolution to map all raster cells within  
679 the study area ( $N$  cells = 518,205) that had similar climatic conditions in the resurvey period compared to  
680 a plot's climate in the baseline period. Climate 'analogy' was assessed by testing, for each bioclimatic  
681 variable separately, whether the climatic variation of any location in the resurvey period could be drawn  
682 from the same distribution as the climate variation for a given plot in the baseline period using non-  
683 parametric two-sample Wilcoxon rank sum tests. We considered significant differences ( $p < .05$ ) as novel  
684 climates and non-significant differences ( $p \geq .05$ ) as analogue climates. Climate analogues were finally  
685 assessed by overlaying the climate analogue areas for each bioclimatic variable separately (see example in  
686 **Fig. S2**).

687 The velocity of climate change was subsequently calculated as the geographic distance (in *km*) between the  
688 plot's coordinates and the cell coordinates of the nearest climate analogue, divided by the time interval.  
689 Quantifying the velocity of climate change based on the nearest climate analogue methods is particularly  
690 useful in the context of this study, as climate analogue shifts are conceptually identical to biotic centroid  
691 shifts: estimates of the absolute velocity of climate change ( $km\ year^{-1}$ ), as well as the projected velocities  
692 along the south-north ( $km\ north\ year^{-1}$ ) and west-east ( $km\ east\ year^{-1}$ ) axes were obtained by using the exact  
693 formulas as the ones used to estimate the rate of centroid shifts. The directionality of climate analogue shifts  
694 was quantified based on the Rayleigh's  $r$  statistic.

695 The calculation of climate change velocities was performed in R making use of the packages *raster* (47)  
696 and *geosphere* (Hijmans 2019). Parallel computation was implemented using the R packages *foreach* (48)  
697 and *doParallel* (49). Maps were produced using the R package *tmap* (50).

698 Note that we here map climate analogues based on statistical testing as an alternative to the classification  
699 of climate analogue mapping based on continuous dissimilarity matrices because (1) it can provide  
700 information on the contribution of each bioclimatic variable separately; and (2) it allows us to consider the  
701 interannual climatic variability (ICV) in both the baseline and resurvey periods, which is biologically very  
702 relevant. For example, locations with stable climatic conditions (with low ICV) are mapped as novel  
703 climatic conditions even under small changes in the climate system, while areas with a highly variable  
704 climates (with large ICV) are more resilient and will not experience biologically relevant changes even  
705 under relatively large oscillations in the climate system.

### 706 3.2. Nitrogen and sulphur deposition rate

707 We quantified the nitrogen (N) and sulphur (S) deposition rates for each plot using the EMEP gridded  
708 database ([https://emep.int/mscw/mscw\\_moddata.html](https://emep.int/mscw/mscw_moddata.html)), providing modelled nitrogen and sulphur

709 deposition data at 0.1° native resolution (~8 km × 8 km within the study area). For each plot in the vegetation  
710 network, the rate of nitrogen (oxidized and reduced) and sulphur (oxidized) deposition was quantified as  
711 the total wet and dry deposition (dry deposition accounted for deciduous temperate forest surface) between  
712 the baseline survey and the resurvey, divided by the inter-survey time interval (expressed in total  $kg\ ha^{-1}$   
713  $year^{-1}$ ). Values of annual nitrogen deposition before the year 1990 were obtained based on the reference  
714 year 2000 and corrected for the time period using the period-specific correction factors published in (51).  
715 Yearly values of nitrogen depositions from 1990 onwards were directly retrieved from the EMEP data  
716 bases. Sulphur and nitrogen deposition contribute to the acidifying deposition rate. This rate (calculated as:  
717  $kg\ N\ ha^{-1}\ year^{-1}/14 + (kg\ S\ ha^{-1}\ year^{-1}/32.06) \times 2$ ,  $Keq\ ha^{-1}\ year^{-1}$ ) was very strongly correlated  
718 (Spearman correlation: 0.87) to the nitrogen deposition rate across all 2,954 plots due to partially shared  
719 emission sources.

### 720 3.3. Rate of forest canopy cover change

721 For each plot in the study area, forest canopy structure was quantified *in situ* as the total cover of the tree  
722 canopies (>7 m) in the baseline survey and resurvey based on visual estimations. Species-specific tree cover  
723 estimates were summed in each plot. The rate of forest canopy cover change was quantified by subtracting  
724 the total canopy cover in the resurvey period from the total canopy cover in the baseline survey divided by  
725 the inter-survey time interval (*percentage canopy cover increase year<sup>-1</sup>*).

### 726 3.4. Nitrogen and acidity (reaction) niche width

727 Species' nitrogen and acidity (reaction) niche width values were extracted from the EIVE-database (32),  
728 presenting ecological indicator values in European plant species (a numerical index between zero and ten;  
729 with higher values indicating more generalist species). The niche width metrics are continuous measures  
730 bounded between 0 and 10 that integrates the intra-regional and inter-regional variability in each species'  
731 nitrogen and acidity niche. In contrast to classical Ellenberg indicator values, which describe niche optima  
732 on ordinal scales, niche width data extracted from the EIVE-data base (32) have several important  
733 advantages for this study: (i) species with a more narrow nitrogen niche tend to be more specialized (33);  
734 (ii) the biogeographical implication is that species with a larger niche width often also have larger ranges  
735 (33); (iii) the continuous nature of the index facilitates its use within conventional linear mixed-effects  
736 modelling.

737

## 738 4. Statistical modeling

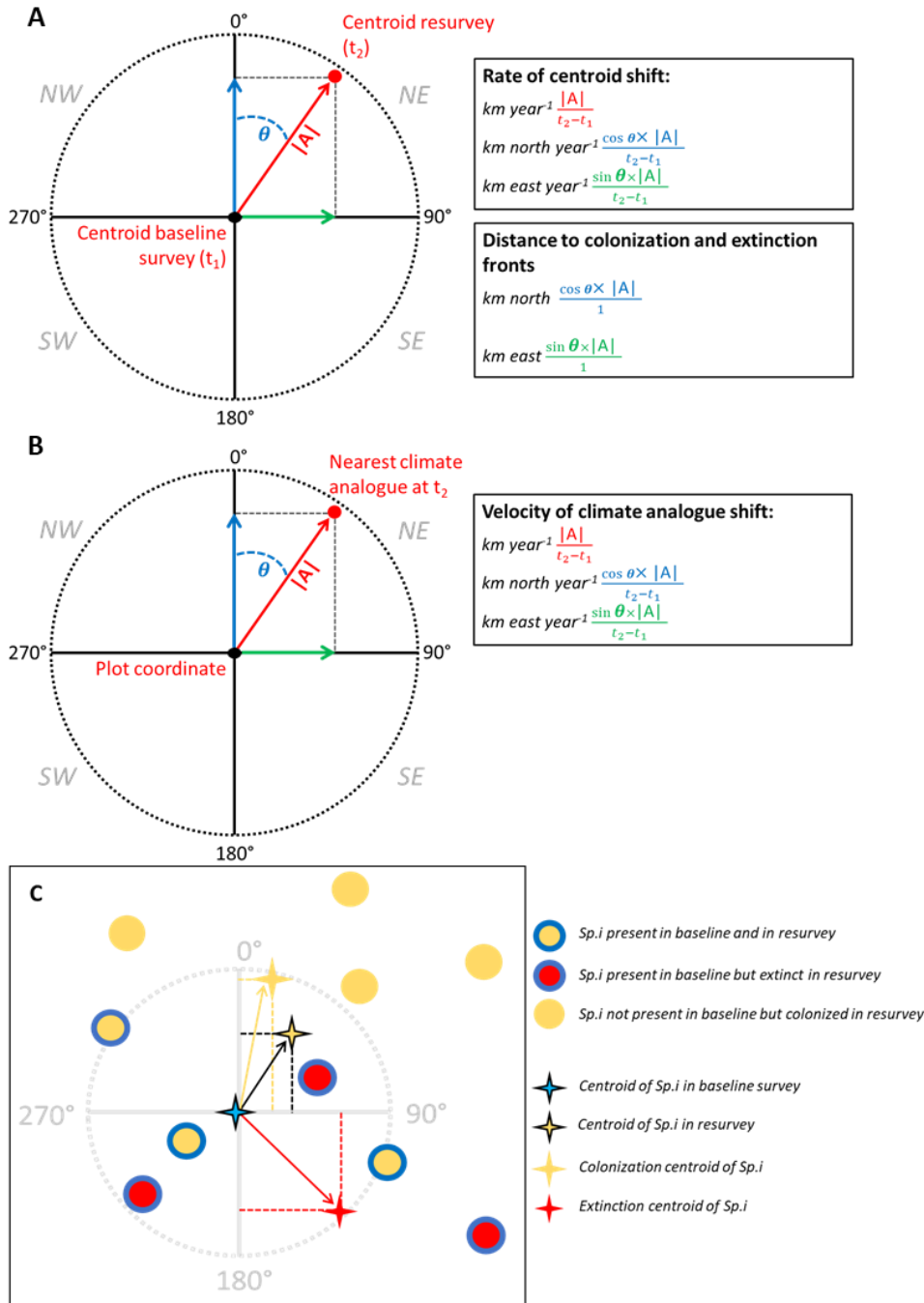
739 4.1. Linear mixed-effects models

740 We ran a set of linear mixed-effects models (LMM) to relate (i) the rate of centroid shifts (absolute, south-  
741 north and west-east rate) and (ii) the northward and eastward distance of colonization and extinction  
742 centroids to three global environmental change drivers that are expected to potentially alter range dynamics  
743 in understory species (1, 14, 16, 52): the velocity of climate change (the absolute velocity [ $km\ year^{-1}$ ], and  
744 the projected south-north and west-east velocity [ $km\ north\ year^{-1}$  and  $km\ east\ year^{-1}$ ]), the nitrogen  
745 deposition rate ( $kg\ N\ ha^{-1}\ year^{-1}$  of reduced and oxidized wet and dry deposition of nitrogen) and the rate of  
746 forest canopy cover change ( $\% canopy\ cover\ increase\ year^{-1}$ ). The LMMs included all possible two-way  
747 interactions and accounted for plant growth form (random intercept, including five levels: forbs,  
748 graminoids, pteridophytes, shrubs and trees) as a random intercept and were conducted with the R package  
749 *lme4* (53). Because centroid shifts are quantified in a species-specific manner while predictor variables  
750 describe the environment at the plot-level, we calculated species-specific abundance-weighted mean values  
751 for each predictor to match the observational unit of the model (i.e., the average environmental change  
752 values across all plots where species *sp<sub>i</sub>* occurred, weighted for its original abundance (12); see **Fig. S6** for  
753 a data flow chart). The absolute velocity of biotic centroid shifts and the absolute velocity of climate  
754 analogue shifts were square root transformed to obtain normality. Pairwise Spearman correlations ( $r$ ) among  
755 the environmental change predictors were acceptable (median  $|r| = 0.09$ ; maximum  $|r| = 0.46$  for nitrogen  
756 deposition rate and the absolute velocity of climate change) (54). For each model, we selected the most  
757 parsimonious (based on Akaike information criterion with small-sample correction [AICc]) using the R  
758 package *MuMIn* (55), with the restricted maximum likelihood argument to 'FALSE'. Once the best model  
759 structure was selected, we set the restricted maximum likelihood argument to 'TRUE' for exact coefficient  
760 estimation (53). Model coefficient estimates (mean values) and 95% confidence intervals (2.5 and 97.5  
761 percentiles) were generated by iterating the single best model structure on 1,000 bootstrap samples.  
762 Significance was considered when the 95% confidence interval did not include zero. Model fit was assessed  
763 as the percentage of variance explained by the fixed effects (marginal  $R^2$ ;  $R^2_m$ ) and the percentage of  
764 variance explained by both fixed and random effects (conditional  $R^2$ ;  $R^2_c$ ) following (56). Prior to  
765 modelling, all predictor variables were  $z$ -transformed to allow a better comparison of the predictors' effect  
766 sizes.

767 To test whether the colonization centroids were associated to the species nitrogen and acidity niche width  
768 and the rates of atmospheric (nitrogen and acidifying, respectively) deposition (and their respective pairwise  
769 interaction effects), we ran a LMM with plant growth form as a random intercept term. The most  
770 parsimonious model was selected as described above.

771 4.2. Variation partitioning

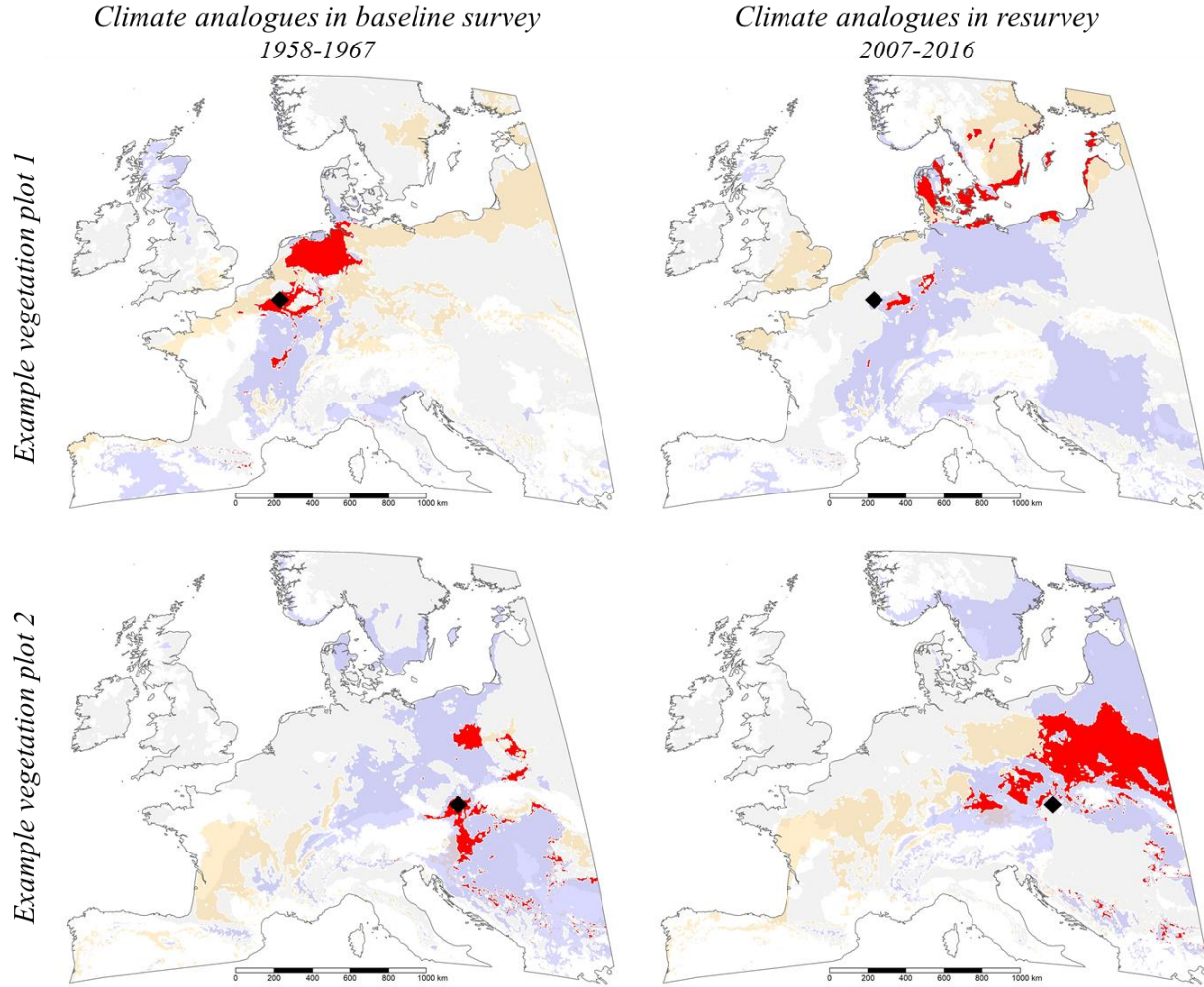
772 In a final step, the unique contribution of each of the three environmental change variables to the full model  
773 was analysed in a variation partitioning analysis. To obtain the variation explained uniquely by each focal  
774 environmental change variable, we subtracted the variation explained by the fixed effects (marginal  $R^2$ ;  
775  $R^2_m$ ) of the partial model, i.e., the full model minus one (out of the three) focal environmental change  
776 predictor variables, from the variation explained by the fixed effects in the full model. The procedure was  
777 repeated on 1,000 bootstrap replicates and the average proportion variation explained (average  $R^2_m$ ) and  
778 95% confidence intervals were calculated. All analyses were performed in R version 4.2.2 (57)



780

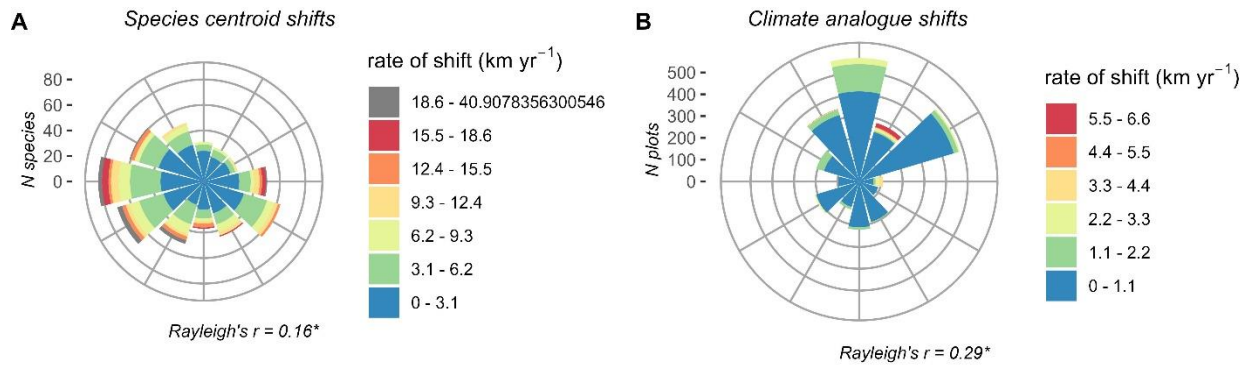
781 **Figure S1 | Schematic illustration of centroid shifts and climate analogue shifts.** (A) Schematic  
 782 overview and calculation of the rate of centroid shifts. (B) Schematic overview and calculation of the  
 783 velocity of climate change based on climate analogue shifts. (C) Conceptual framework and definition of  
 784 centroid shifts, colonization and extinction centroids for a certain species (sp.i). From a biogeographical  
 785 point of view, longer distances reflect that colonization or local extinction events took place farther away

786 from the baseline centroid, suggesting that these processes are happening in a preferred direction relative  
787 to the baseline centroid position.



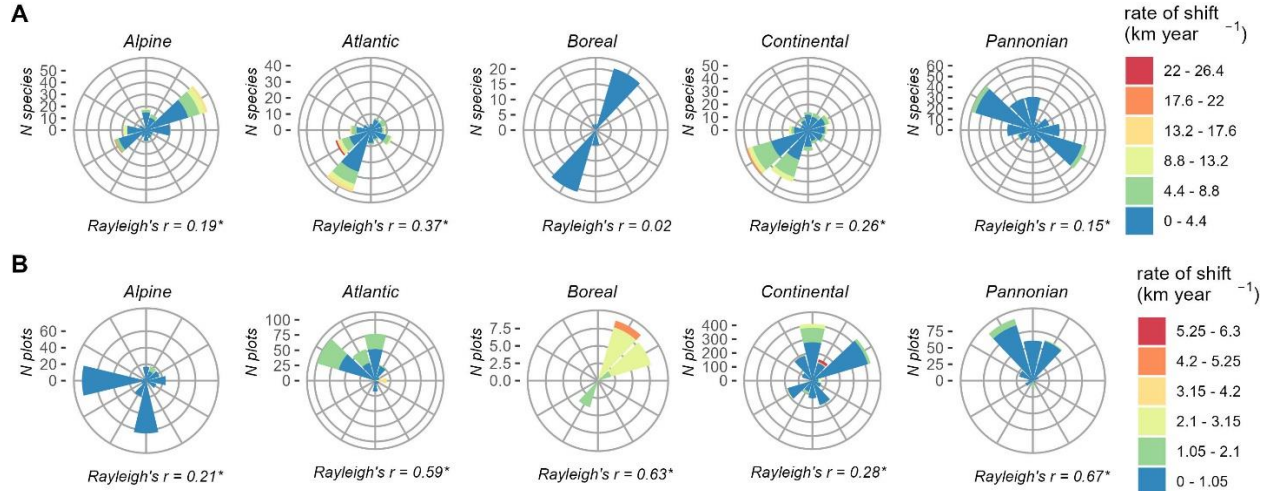
788

789 **Figure S2 | Climate analogue mapping integrating three bioclimate variables.** Climate analogue  
 790 mapping at  $4 \text{ km} \times 4 \text{ km}$  resolution for the climatic conditions in the baseline (average climate values in  
 791 the period 1958-1967) and resurvey period (average climate values in the period 2007-2016) in two  
 792 vegetation plots. Climate analogues for a given plot (black square) in the baseline period (left) and shifts in  
 793 climate analogues in the resurvey relative to the climatic conditions in the baseline period (right) for three  
 794 bioclimate variables separately: maximum growing-season temperatures (orange), minimum winter  
 795 temperatures (blue) and total growing-season precipitation (grey), and the overlaid climate analogue areas  
 796 of all three bioclimatic variable together (red). The velocity of climate change was calculated as the distance  
 797 to the nearest climate analogue raster cell (thus, within the red area) over time.

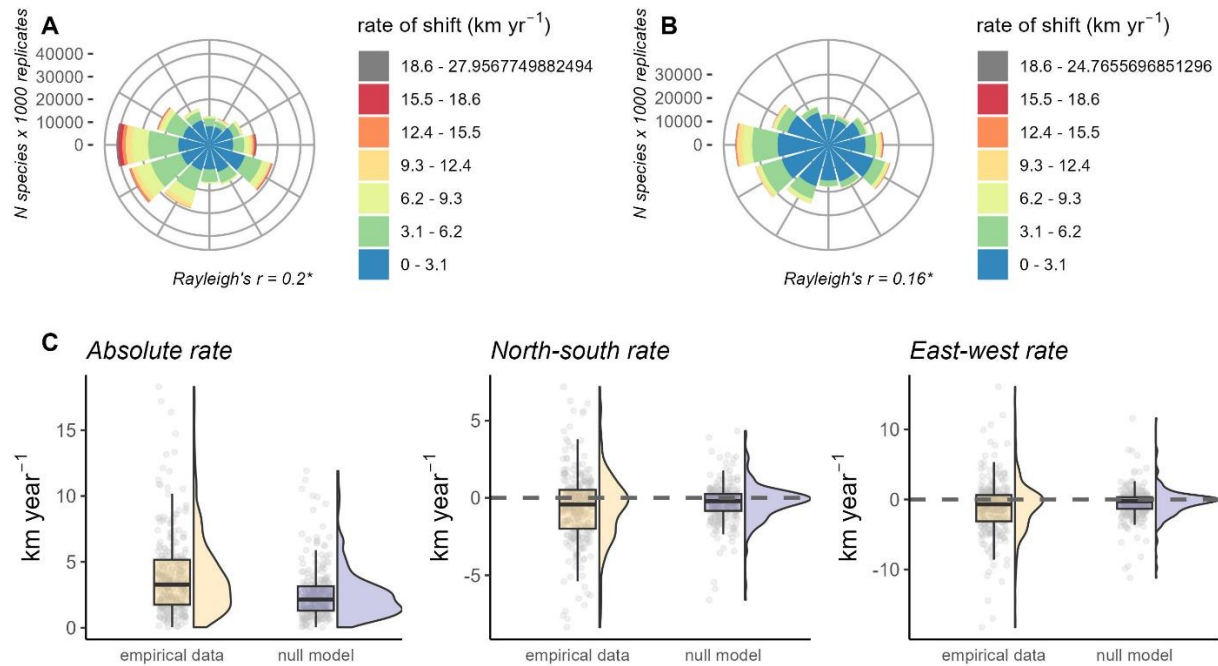


798  
799  
800  
801  
802  
803  
804

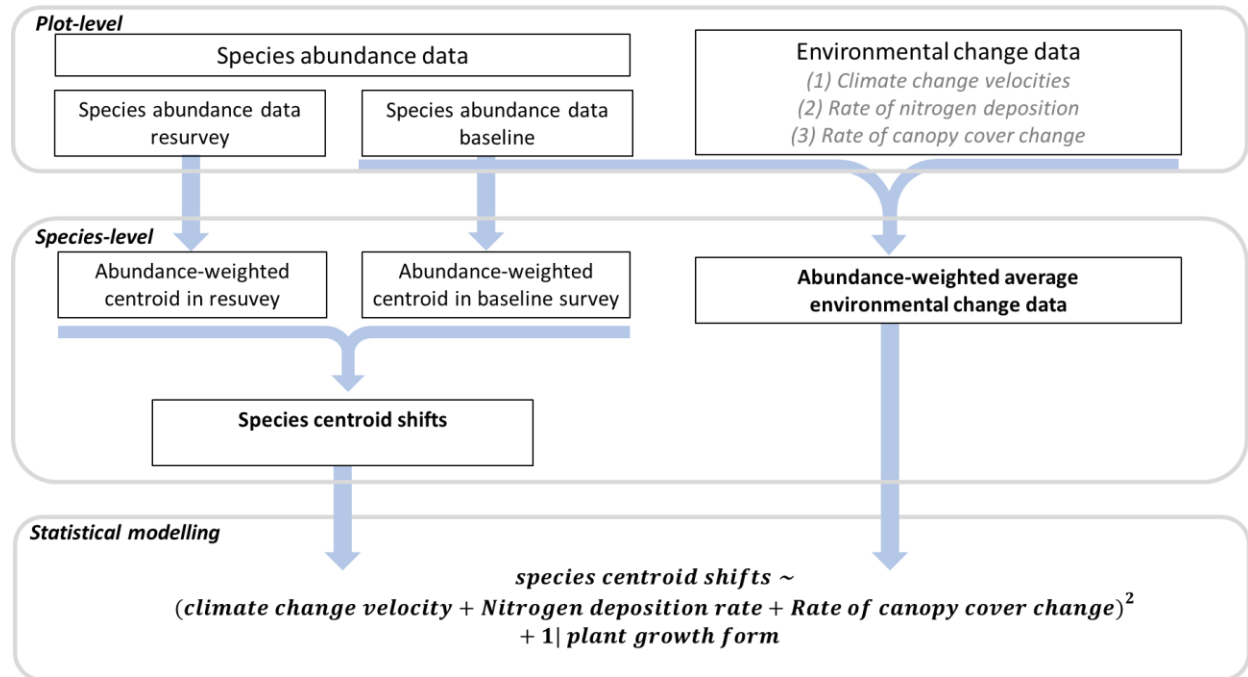
**Figure S3 | Rate and geographic direction of centroid shifts and climate analogue shifts.** (A) Rate and geographic direction of species centroid (including rare species;  $n$  species = 596). (B) Rate and geographic direction climate analogue shifts ( $n$  plots = 2,954). In all graphs, the Rayleigh's  $r$  statistic represents a test of uniformity that compares the bearings of shifts to a uniform circular distribution (null hypothesis). Larger values indicate more directional shifts. Asterisk (\*) indicates significant deviations from the null hypothesis ( $p < 0.05$ ).



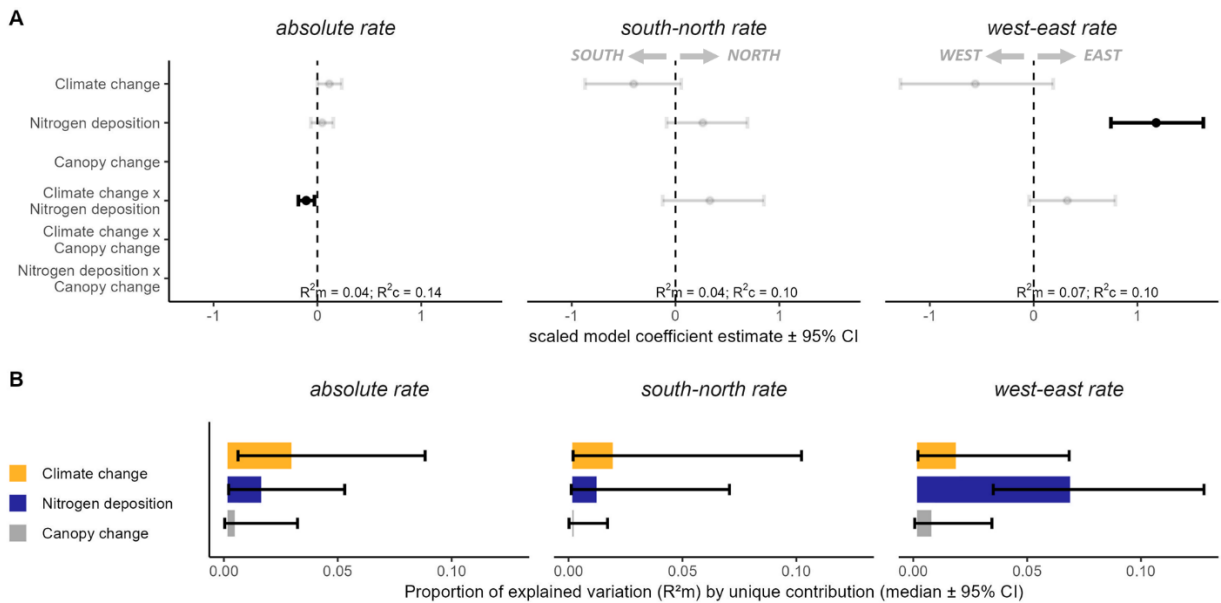
805  
 806 **Figure S4 | Rate and geographic direction of centroid shifts and climate analogue shifts per**  
 807 **biogeographic region.** (A) Rate and bearing of species centroid shifts ( $n$  species Alpine = 173; Atlantic =  
 808 144; Boreal = 41; Continental = 225; Pannonian = 256). (B) Rate and bearing of climate analogue shifts ( $n$   
 809 plots Atlantic = 322; Alpine = 266; Boreal = 21; Continental = 2049; Pannonian = 296). Rayleigh's  $r$   
 810 statistic represents a test of uniformity that compares the bearings of shifts to a uniform circular distribution  
 811 (null hypothesis). Larger values indicate more directed shifts. Asterisk (\*) indicates significant deviations  
 812 from the null hypothesis ( $p < 0.05$ ). Biogeographical boundaries were defined by the European  
 813 Environment Agency ([www.eea.europa.eu](http://www.eea.europa.eu)).



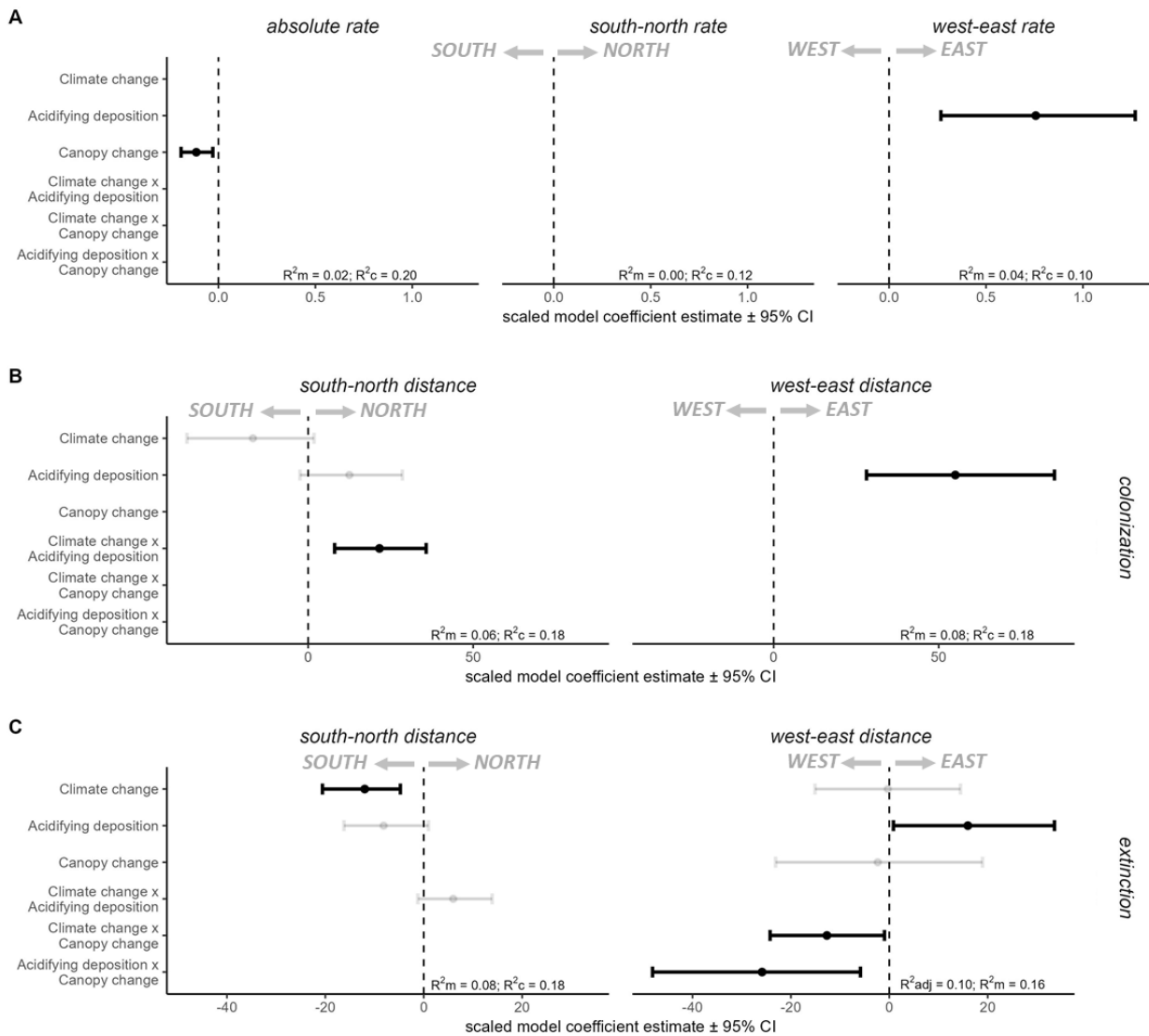
814  
 815 **Figure S5 | Rate and geographical direction of centroid shifts that can be attributed to random noise**  
 816 **due to the plot distribution.** (A) Rate and geographic direction of species centroids for 1,000 bootstrapped  
 817 replicates ( $n$  species =  $266 \times 1,000$  replicates). (B) Rate and geographic direction of null models where  
 818 species-specific abundances were randomized across all plots in which the species was observed, and  
 819 resampled 1,000 times ( $n$  species =  $266 \times 1,000$  replicates). In all graphs, the Rayleigh's  $r$  statistic represents  
 820 a test of uniformity that compares the bearings of shifts to a uniform circular distribution (null hypothesis).  
 821 Larger values indicate more directional shifts. Asterisk (\*) indicates significant deviations from the null  
 822 hypothesis ( $p < 0.05$ ). (C) Comparison between species-specific bootstrapped estimates and null models of  
 823 the absolute rate and the south-north and west-east rate (grey symbols; average across 1,000 replicates).  
 824 The magnitudes of centroid shifts are significantly different from random noise owing to the spatial  
 825 distribution of the vegetation plots by 66% (northward shifts were 66% faster than expected based on  
 826 random movements), 62% (southward shifts), 63% (westward shifts) and 70% (eastward shifts).



827  
 828 **Figure S6 | Framework of the study and flow chart of the data.** Species abundance data were collected  
 829 at the plot-level during a baseline and resurvey period. Environmental change data were collected at the  
 830 plot-level. Species-specific abundance-weighted centroids were calculated for the baseline survey and the  
 831 resurvey. The rate of centroid shift was calculated as the absolute rate, the projected south-north and west-  
 832 east rate, and the northward and eastward distance of colonization and extinction centroids. Species-specific  
 833 environmental change data were obtained by taking the average environmental change values (realized  
 834 change between the baseline and resurvey period) in all plots where the species was observed in the baseline  
 835 period, weighted by its original abundance. Using linear mixed-effects models, biotic centroid shifts were  
 836 linked to the abundance-weighted environmental change data and all pairwise interactions (indicated by <sup>2</sup>).  
 837 Plant growth form (with five levels: forbs, graminoids, pteridophytes, shrubs and trees) was included as a  
 838 random effect term in all models.

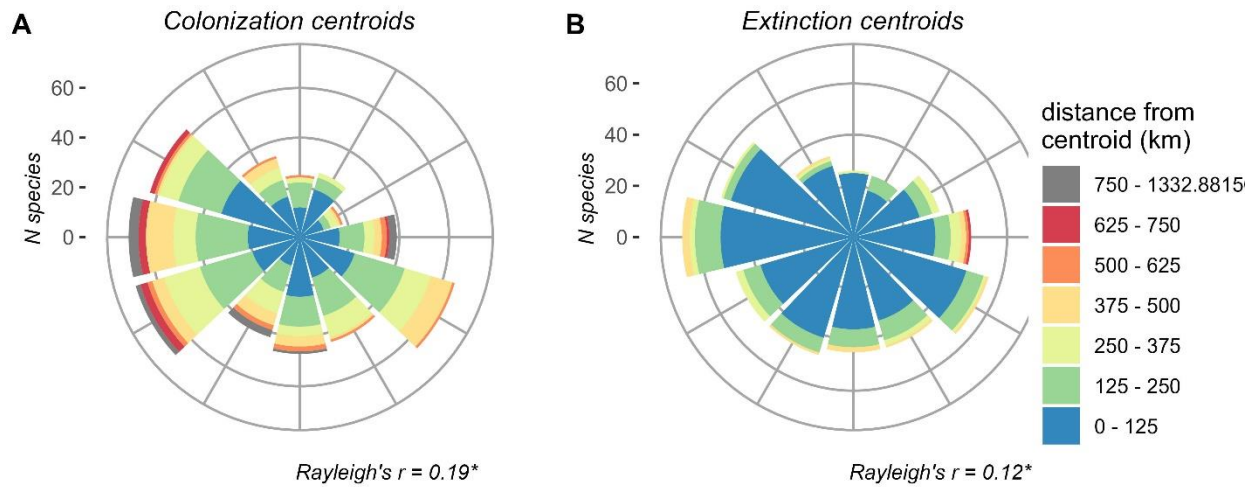


839  
840 **Figure S7 | Effects of environmental changes on centroid shifts based on the most parsimonious**  
841 **model, including rare species.** (A) Results of the mixed effect models (including rare species;  $n$  species =  
842 596) indicating coefficient estimates and 95% confidence intervals (CI) of the effects of velocity of climate  
843 change ( $km\ year^{-1}$ ,  $km\ north\ year^{-1}$ ,  $km\ east\ year^{-1}$ ), average nitrogen deposition rate between the baseline  
844 survey and resurvey ( $kg\ N\ ha^{-1}\ year^{-1}$ ), and canopy change ( $\% cover\ increase\ year^{-1}$ ), and all pairwise  
845 interactions (indicated by ‘x’) on the absolute rate of centroid shifts ( $km\ north\ year^{-1}$ ; negative values  
846 indicate southward shifts) and west-east rate ( $km\ east\ year^{-1}$ ; negative values indicate westward shifts)  
847 extracted from the most parsimonious model (empty rows were not included in the final selected model).  
848 All the predictor variables are  $z$ -transformed to increase comparability. Model fit is presented as the  
849 proportional explained variation by the fixed effect (marginal  $R^2$ ,  $R^2_m$ ) and the proportional explained  
850 variation by the fixed and random effects (conditional  $R^2$ ,  $R^2_c$ ). Models accounted for plant growth form as  
851 random effect (five levels: forbs, graminoids, pteridophytes, shrubs and trees); (B) Results of the variation  
852 partitioning analyses representing the individual contribution of each environmental predictor. Bar plots  
853 are proportional to the explained variation by the unique contribution of each fixed effect (expressed as  
854  $R^2_m$ ). In all graphs, estimates and error bars represent the median value and 2.5 – 97.5 percentiles across  
855 1,000 bootstrap samples.



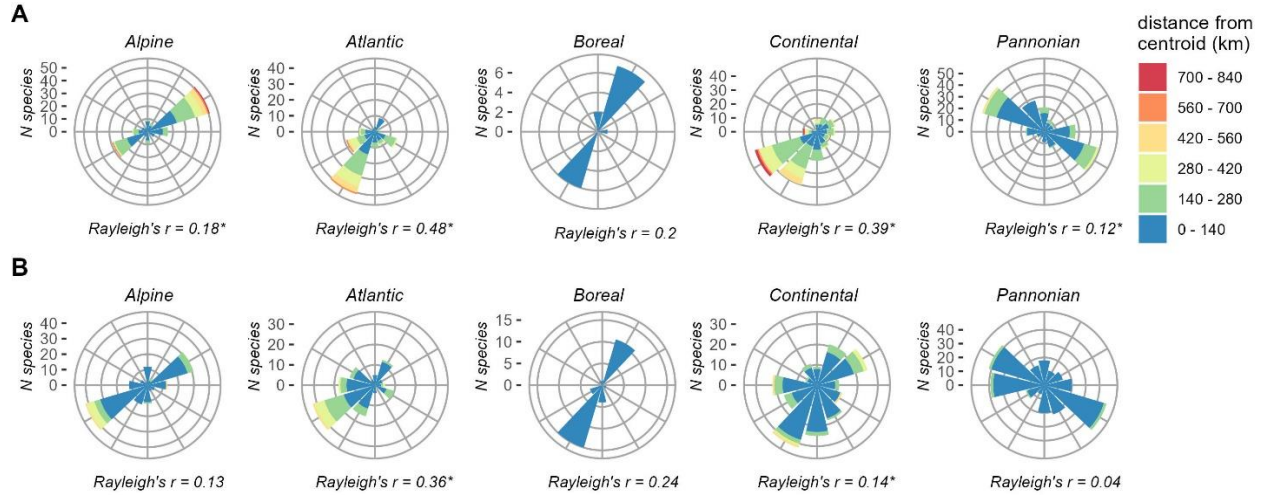
856  
857 **Figure S8 | Effects of environmental changes on the rate of centroid shifts (A), distance of colonization**  
858 **(B) and extinction (C) centroids based on the most parsimonious model. (A)** Results of the mixed-  
859 effects models ( $n$  species = 266) indicating coefficient estimates and 95% confidence intervals (CI) of the  
860 effects of velocity of climate change ( $km$  north  $year^{-1}$ ,  $km$  east  $year^{-1}$ ), average acidifying deposition rate  
861 between the baseline and resurvey ( $Keq$   $ha^{-1}$   $year^{-1}$ ), and canopy change ( $\%$  cover increase  $year^{-1}$ ), and all  
862 pairwise interactions (indicated by ‘x’) on the absolute rate, south-north rate ( $km$  north  $year^{-1}$ ; negative  
863 values indicate southward shifts) and west-east rate ( $km$  east  $year^{-1}$ ; negative values indicate westward  
864 shifts) of centroids shifts extracted from the most parsimonious model (empty rows were not included in  
865 the final selected model). **(B, C)** Results of the mixed-effects models ( $n$  species = 202 and 246 for  
866 colonization and extinction centroids, respectively) indicating coefficient estimates (95% CI) of the  
867 environmental changes on south-north and west-east distance of colonization extinction centroids extracted  
868 from the most parsimonious model. In all graphs, estimates and error bars represent the median value and  
869 2.5 – 97.5 percentiles across 1,000 bootstrap samples. Bar plots are proportional to the variation explained  
870 by the unique contribution of each fixed effect (expressed as  $R^2_m$ ). Model fit is presented as the proportion  
871 variation explained by the fixed effect (marginal  $R^2$ ,  $R^2_m$ ) and the proportion variation explained by the

872 fixed and random effects (conditional  $R^2$ ,  $R^2_c$ ). Models accounted for plant growth form as random effect  
873 (five levels: forbs, graminoids, pteridophytes, shrubs and trees). All the predictor variables were z-  
874 transformed to increase comparability.

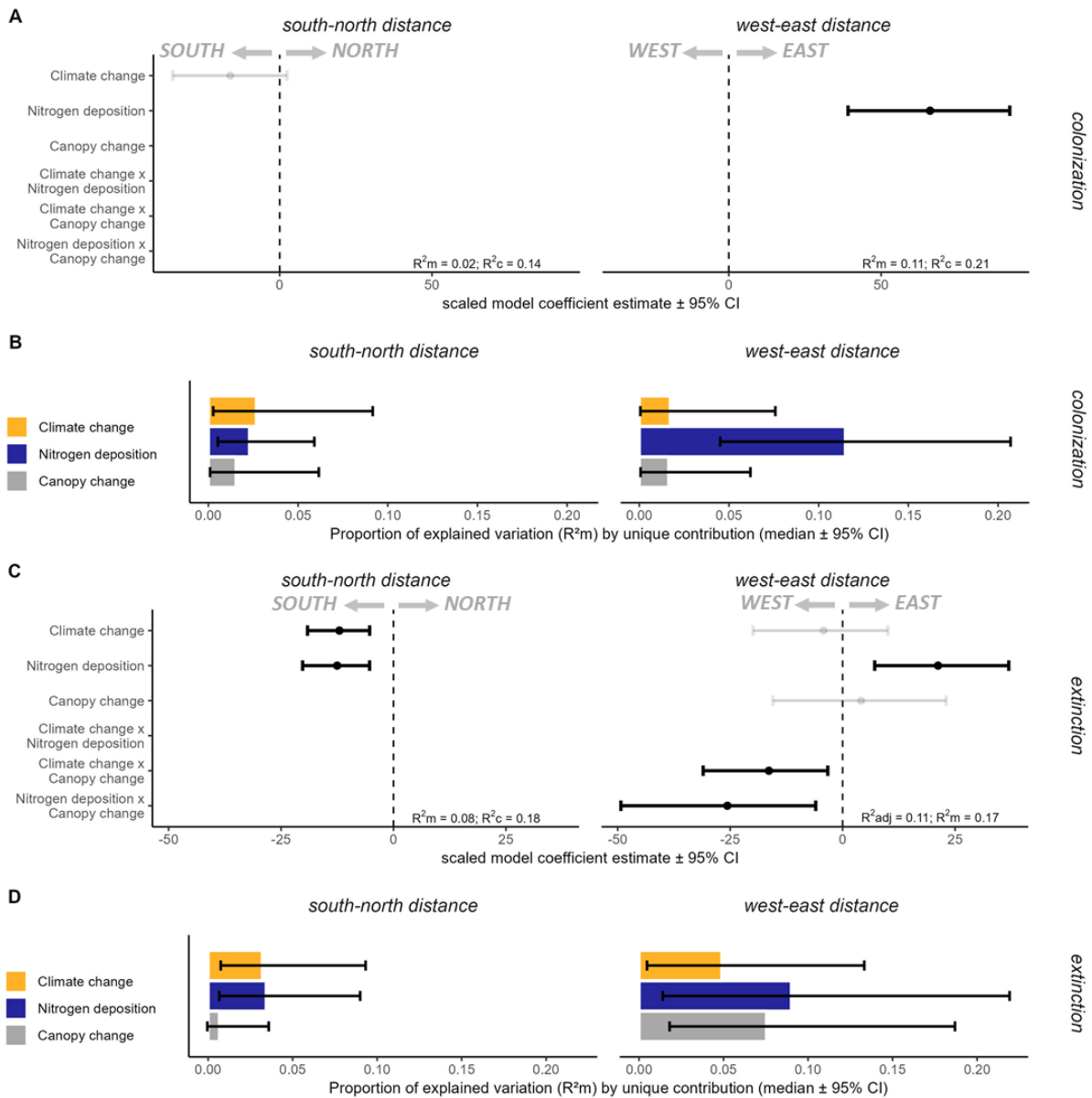


875  
876  
877  
878  
879  
880  
881  
882

**Figure S9 | Distance and geographic direction of colonization and extinction centroids accounted for rare species.** (A) Distance and geographic direction of colonization centroids (including rare species;  $n$  species = 542). (B) Distance and geographic direction of extinction centroids ( $n = 527$ ). Longer distances reflect that colonization or extinction took place further away from the original centroid and that these processes are happening in a preferred direction. Rayleigh's  $r$  statistic represents a test of uniformity that compares the bearings of shifts to a uniform circular distribution (null hypothesis). Larger values indicate more directed shifts. Asterisk (\*) indicates significant deviations from the null hypothesis ( $p < 0.05$ ).

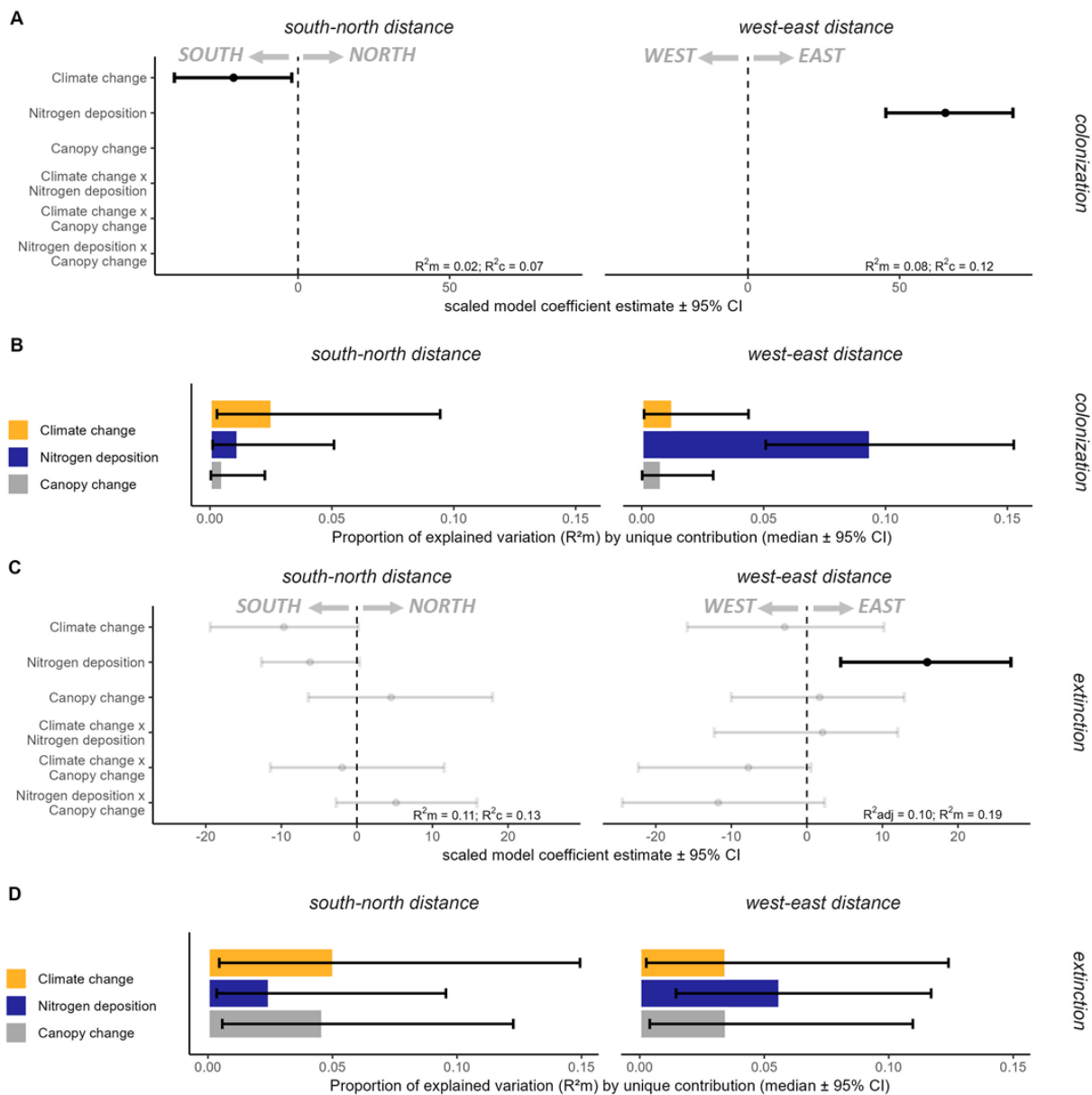


883  
 884 **Figure S10 | Distance and geographic direction of colonization and extinction centroids for each**  
 885 **biogeographic region. (A)** Distance and bearing of colonization centroids ( $n$  species Alpine = 130; Atlantic  
 886 = 126; Boreal = 7; Continental = 193; Pannonian = 212). **(B)** Distance and bearing of extinction centroids  
 887 ( $n$  species Alpine = 140; Atlantic = 125; Boreal = 28; Continental = 211; Pannonian = 250). Rayleigh's  $r$   
 888 statistic represents a test of uniformity that compares the bearings of shifts to a uniform circular distribution  
 889 (null hypothesis). Larger values indicate more directed shifts. Asterisk (\*) indicates significant deviations  
 890 from the null hypothesis (at the level of  $p < 0.05$ ). Biogeographical boundaries were defined by the  
 891 European Environment Agency ([www.eea.europa.eu](http://www.eea.europa.eu)).



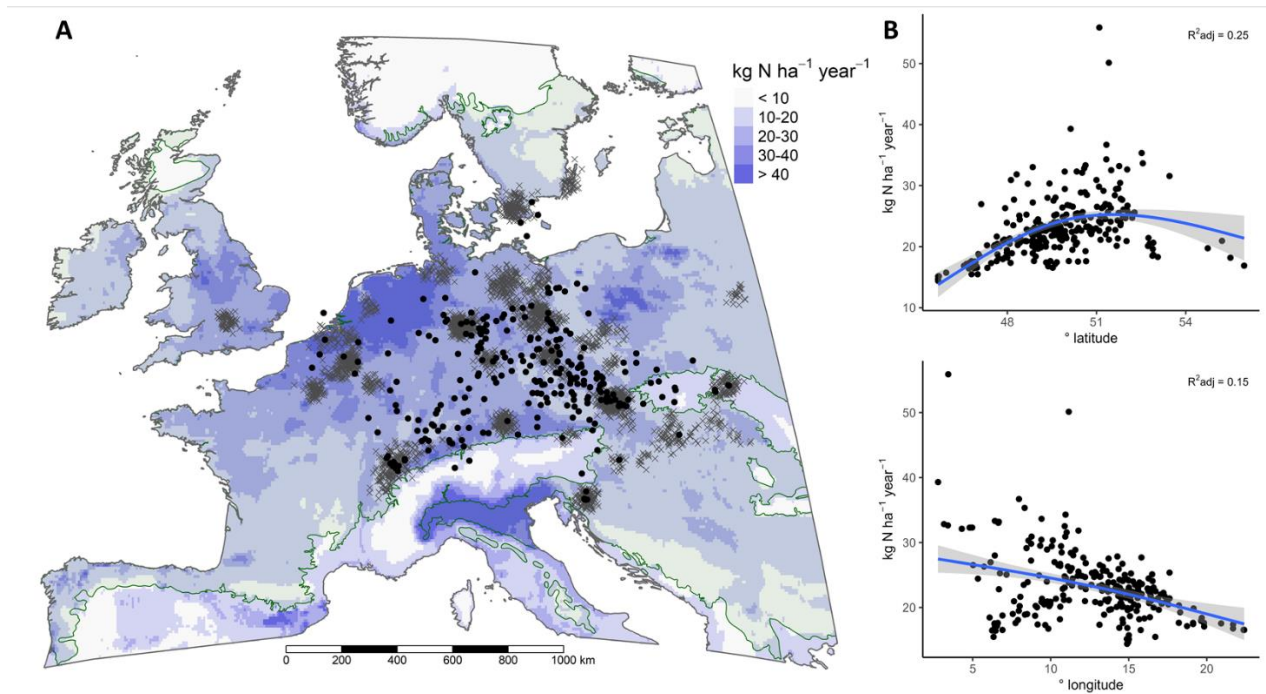
892  
893 **Figure S11 | Effects of environmental changes on the distance of colonization and extinction centroids**  
894 **based on the most parsimonious model.** (A–B) Results of the mixed-effects models ( $n$  species = 202)  
895 indicating coefficient estimates and 95% confidence intervals (CI) of the effects of velocity of climate  
896 change ( $km$  north year<sup>-1</sup>,  $km$  east year<sup>-1</sup>), average nitrogen deposition rate between the baseline and resurvey  
897 ( $kg$  N ha<sup>-1</sup> year<sup>-1</sup>), and canopy change (% cover increase year<sup>-1</sup>), and all pairwise interactions (indicated by  
898 ‘x’) on northward ( $km$  north; negative values indicate southward colonization) and eastward distance ( $km$   
899 east; negative values indicate westward colonization) of colonization centroids extracted from the most  
900 parsimonious model (empty rows were not included in the final selected model), and output of the variation  
901 partitioning analysis representing the individual contribution of each environmental predictor. The results  
902 show that westward colonization was more common in species that have experienced a lower rate of  
903 nitrogen deposition across their distribution. (C–D) Results of the mixed-effects models ( $n$  species = 246)  
904 indicating coefficient estimates (95% CI) of the effects of velocity of climate change, average nitrogen

905 deposition rate between the baseline and resurvey, and canopy change, and all pairwise interactions on  
906 northward and eastward distance of extinction centroids extracted from the most parsimonious model, and  
907 output of the variation partitioning analysis. The results show that species' southward extinction centroids  
908 were related to the poleward velocity of climate change and high rates of nitrogen deposition. Eastward  
909 extinction centroids were related to a high rate nitrogen deposition and canopy opening. Eastward extinction  
910 owing to climate change was more common under canopy opening. In all graphs, estimates and error bars  
911 represent the median value and 2.5 – 97.5 percentiles across 1,000 bootstrap samples. Bar plots are  
912 proportion to the variation explained by the unique contribution of each fixed effect (expressed as  $R^2_m$ ).  
913 Model fit is presented as the proportional explained variation by the fixed effect (marginal  $R^2$ ,  $R^2_m$ ) and the  
914 proportion variation explained by the fixed and random effects (conditional  $R^2$ ,  $R^2_c$ ). Models accounted for  
915 plant growth form as random effect (five levels: forbs, graminoids, pteridophytes, shrubs and trees). All the  
916 predictor variables were  $z$ -transformed to increase comparability. See **Fig. S12** for results on the analyses  
917 that also included rare species.



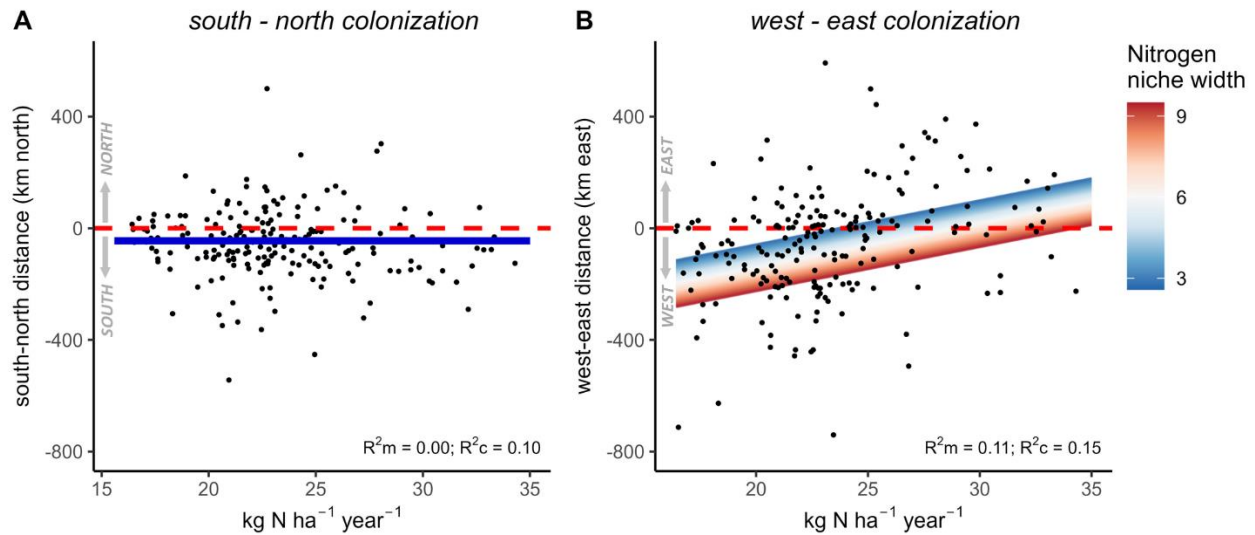
918  
 919 **Figure 12 | Effects of environmental changes on the distance of colonization and extinction centroids**  
 920 **based on the most parsimonious model, including rare species.** (A-B) Results of the mixed-effect  
 921 models (including rare species;  $n$  species = 542) indicating coefficient estimates and 95% confidence  
 922 intervals (CI) of the effects of velocity of climate change ( $km$  north  $year^{-1}$ ,  $km$  east  $year^{-1}$ ), average nitrogen  
 923 deposition rate between the baseline and resurvey ( $kg$   $N$   $ha^{-1}$   $year^{-1}$ ), and canopy change ( $\%$  cover increase  
 924  $year^{-1}$ ), and all pairwise interactions (indicated by 'x') on northward ( $km$  north; negative values indicate  
 925 southward colonization) and eastward distance ( $km$  east; negative values indicate westward colonization)  
 926 of colonization centroids extracted from the most parsimonious model (empty rows were not included in  
 927 the final selected model), and output of the variation partitioning analysis representing the individual  
 928 contribution of each environmental predictor. (C-D) Results of the mixed-effects models (including rare  
 929 species;  $n$  species = 527) indicating coefficient estimates (95% CI) of the effects of velocity of climate  
 930 change, average nitrogen deposition rate between the baseline and resurvey, and canopy change, and all

931 pairwise interactions on northward and eastward distance of extinction centroids extracted from the most  
932 parsimonious model (empty rows were not included in the final selected model), and output of the variation  
933 partitioning analysis. In all graphs, estimates and error bars represent the median value and 2.5 – 97.5  
934 percentiles across 1,000 bootstrap samples. Bar plots are proportional to the explained variation by the  
935 unique contribution of each fixed effect (expressed as  $R^2_m$ ). Model fit is presented as the proportion of  
936 explained variation by the fixed effect (marginal  $R^2$ ,  $R^2_m$ ) and the proportion of explained variation by the  
937 fixed and random effects (conditional  $R^2$ ,  $R^2_c$ ). Models accounted for plant growth form as random effect  
938 (five levels: forbs, graminoids, pteridophytes, shrubs and trees); All the predictor variables are  $z$ -  
939 transformed to increase comparability.

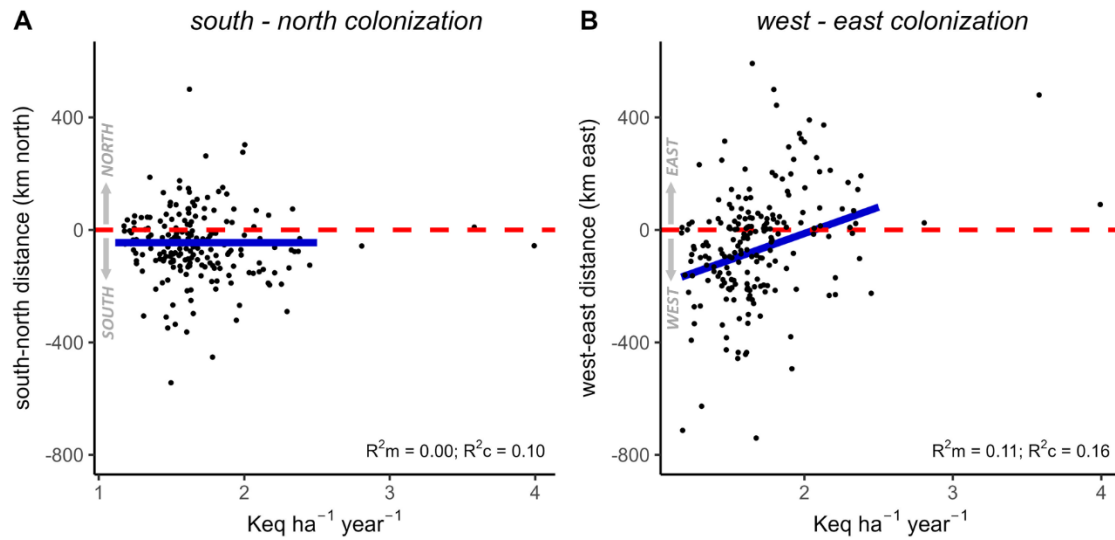


940  
941  
942  
943  
944  
945  
946  
947  
948

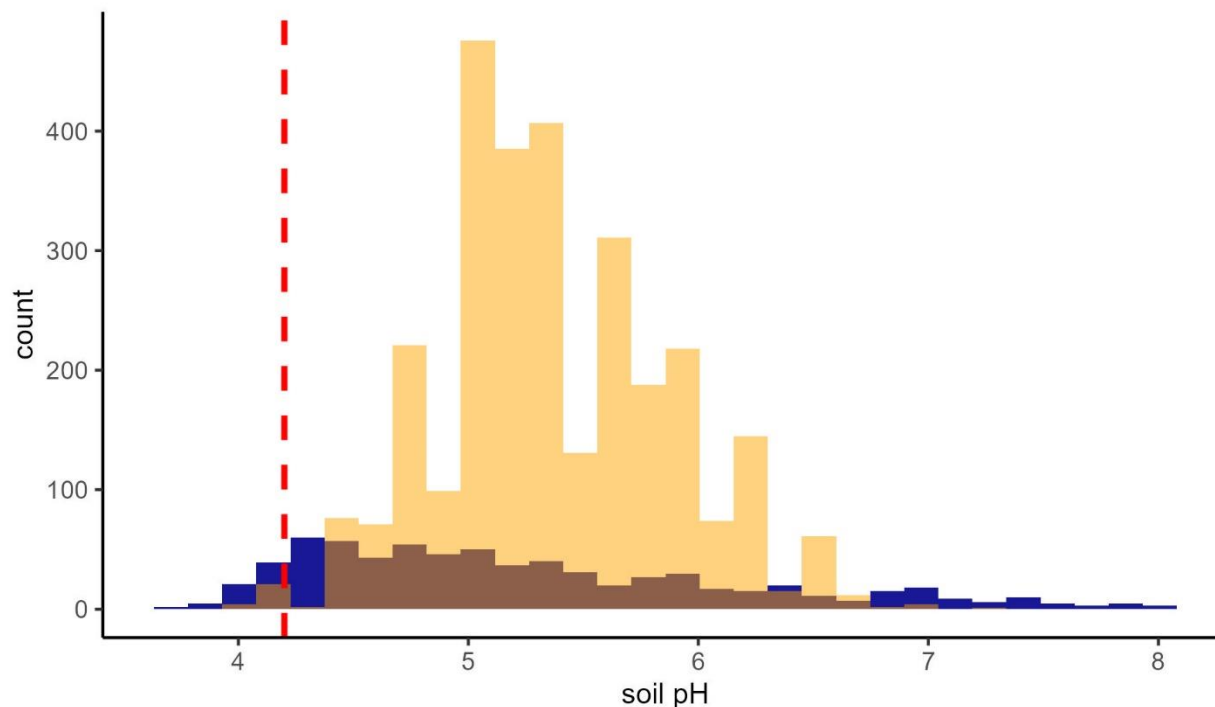
**Figure S13 | Spatial variation in the nitrogen deposition rate across the baseline centroid positions.** (A) Map of modelled nitrogen (N) deposition rate (sum oxidized and reduced wet and dry deposition expressed in  $\text{kg N ha}^{-1} \text{ year}^{-1}$ ; dry deposition accounted for deciduous forest surface) at  $0.1^\circ$  resolution for the reference year 2000. Black dots indicate the abundance-weighted centroid of the 266 most common species in the data set. Grey crosses indicate the distribution of the 2,954 vegetation plots (spatially jittered for clarity). (B) species-specific abundance-weighted nitrogen deposition rates regressed to the degree ( $^\circ$ ) latitude and longitude of each species' baseline centroid ( $n$  species = 266). The regression line represents the model fit of a generalized additive model, with the k-parameter restricted to three to avoid overfitting.



949  
 950 **Figure S14 | Effects of nitrogen deposition rates and species nitrogen niche width on colonization**  
 951 **centroids based on the most parsimonious model when outlier data points were excluded ( $n = 3$  data**  
 952 **points).** Results of the mixed-effects model testing for the interaction effect between the average nitrogen  
 953 deposition rate across each species' distribution ( $\text{kg N ha}^{-1} \text{ year}^{-1}$ ) and species Ecological Indicator Value  
 954 for nitrogen niche width (an index integrating the intra- and inter-regional variability in the nitrogen niche,  
 955 with higher values indicating more generalist species) on the south-north and west-east colonization  
 956 centroids. Negative distances indicate southward (A) or westward colonization (B). The effects of nitrogen  
 957 niche width is plotted with the color gradient. The most parsimonious model structure for west-east  
 958 colonization did not include the interaction effect anymore, but colonization centroids for generalist species  
 959 were still often more westward. Colonization centroids of specialist species were either west- or eastward,  
 960 depending on the experienced nitrogen deposition rate. The most parsimonious model of south-north  
 961 colonization was an intercept-only model (blue line). Nitrogen generalist species that initially occurred in  
 962 areas with lower rates of nitrogen deposition moved westward. Colonization in the more specialist species  
 963 was equally likely westward or eastward, depending on the average rate of nitrogen deposition across their  
 964 distribution.



965  
 966 **Figure S15 | Model output of the effects of acidifying deposition rates (Keq ha<sup>-1</sup> year<sup>-1</sup>) and species**  
 967 **acidity (reaction) niche width on colonization centroids based on the most parsimonious model.**  
 968 Results of the mixed-effects model testing for the interaction effect between the average acidifying  
 969 deposition rate across each species' distribution (Keq ha<sup>-1</sup> year<sup>-1</sup>) and species Ecological Indicator Value  
 970 for acidity (reaction) niche width (an index integrating the intra- and inter-regional variability in the reaction  
 971 niche) on the south-north and west-east colonization centroids. Negative distances indicate southward (A)  
 972 or westward colonization (B). The acidity niche width was not included in the most parsimonious model  
 973 structure. Colonization centroids of species were mainly westward for species that experienced lower rates  
 974 of acidifying deposition rates. The most parsimonious model of south-north colonization was an intercept-  
 975 only model (blue line).



976  
 977 **Figure S16 | Distribution of the top-soil pH (pH-H<sub>2</sub>O) conditions across the studied vegetation plots.**  
 978 Orange: interpolated top-soil pH (pH-H<sub>2</sub>O) conditions by overlaying all out 2,954 studied vegetation plots  
 979 on top of the gridded soil data layer (SoilGrids.org, 250-meter resolution) available at 250-meter resolution  
 980 globally. Blue: measured top-soil pH (pH-H<sub>2</sub>O) conditions from in-situ soil samples available for 704  
 981 vegetation plots across the study area. In-situ soil pH data is available from (58). The median value of top  
 982 soil pH (pH-H<sub>2</sub>O) levels across the plots was between 5.3 (data SoilGrids.org, n plots = 2,954) 5.04 (in-situ  
 983 soil samples, n plots = 704). The soils across the majority of our plots are relatively well buffered against  
 984 acidifying deposition due to base cation exchange. Only 0.6 % of all plots (8.8% of the subset of plots with  
 985 field data) have soil pH levels below the critical pH level of 4.2, a threshold below in which base cations  
 986 become depleted and levels of Al<sup>+3</sup> increase in the soil solution (59).

987 **Supplementary Data**

988 **Data S1 | Species list and rates of centroid shifts and environmental changes.** Full list of study species  
989 considered, and species-specific values of the absolute rate ( $\text{km year}^{-1}$ ), the south-north rate ( $\text{km north year}^{-1}$ )  
990 and the west-east rate ( $\text{km east year}^{-1}$ ) of centroid shifts; and species-specific experienced rates of  
991 atmospheric (nitrogen and acidifying) deposition ( $\text{kg N year}^{-1} \text{ ha}^{-1}$ ;  $\text{K eq year}^{-1} \text{ ha}^{-1}$ ), forest canopy cover  
992 change ( $\% \text{ cover increase yr}^{-1}$ ) and climate change velocities ( $\text{km yr}^{-1}$ ,  $\text{km north yr}^{-1}$ ,  $\text{km east yr}^{-1}$ ).